

**THE EFFECT OF BOUNDARY LAYER PROFILE,
AIR SPEED, AND SYSTEM GEOMETRY ON THE
STABILITY OF FLOW IN SUCTION SYSTEMS**

C. E. TREANOR

A. H. FLAX

CORNELL AERONAUTICAL LABORATORY, INC.
BUFFALO, NEW YORK

JULY 1956

SEP 14 1956

AERONAUTICAL RESEARCH LABORATORY
CONTRACT AF 33(616)-2373
PROJECT 1366
TASK 70103

WRIGHT AIR DEVELOPMENT CENTER
AIR RESEARCH AND DEVELOPMENT COMMAND
UNITED STATES AIR FORCE
WRIGHT-PATTERSON AIR FORCE BASE, OHIO

Contrails

FOREWORD

The work described in this report was carried out by the Aerodynamic Research Department of the Cornell Aeronautical Laboratory under Air Force Contract AF 33(616)-2373, Expenditure Order No. R470-103-SR 1_z. This contract was administered by the Aeronautical Research Laboratory, Wright Air Development Center, under the technical cognizance of Mr. Anthony W. Fiore. The research is identified as Task 70103 of Project 1366, "External and Internal Aerodynamics."

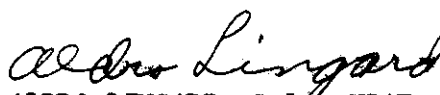
WADC TR 55-318

The stability of flow in air induction systems for boundary-layer suction has been studied as a continuation of the theoretical and experimental work reported in WADC TR 53-189. In these suction systems, the dynamic head of the boundary-layer air can increase the pressure in the suction system, causing dynamic and static instability. The theoretical work reported here extends the previous analysis to include the effects of wave motion in the exit section of the suction system. The experiments include tests with both a turbulent boundary layer and an artificially produced laminar-like boundary layer, obtained by air injection through the tunnel wall. The static instability is evidenced by the appearance of unequal flows in ostensibly identical branches of the system. Inserting splitter vanes in the slot and diffuser accents this instability, the flow confining itself to separate sections of the diffuser for moderate suction rates. Several devices to remove the static instability were unsuccessful, but the use of the laminar-like boundary layer has a strong stabilizing effect. The dynamic instability occurs in the form of regular oscillations in the flow. It was shown in WADC TR 53-189 that the system could be made dynamically stable by introducing large losses in the suction slot. In the present report four stabilizing effects are investigated: small plenum volume, laminar-like boundary layer, large-chord entrance slot, and low tunnel speed. Conditions for dynamic stability are investigated theoretically, and a stability criterion is compared with the experimental results. The experiments with the dynamic instability include measurements of the amplitude and phases of the oscillations in various places in the suction system. An expression is derived for the frequency of oscillation in the case of dynamic instability. The calculated frequency agrees with the experimental measurements for large plenum volume, but is not in agreement for measurements with the small plenum. The energy balance in the dynamically unstable system is investigated theoretically and these results are compared with experiment.

PUBLICATION REVIEW

This report has been reviewed and is approved.

FOR THE COMMANDER:



ALDRO LINGARD, Col, USAF
Chief, Aeronautical Research Laboratory
Directorate of Research

Contrails

TABLE OF CONTENTS

	Page
LIST OF ILLUSTRATIONS	v
LIST OF SYMBOLS	vi
INTRODUCTION	1
THEORETICAL ANALYSIS	3
Boundary-Layer Characteristics	3
Dynamic Characteristics of the Exit Duct	4
Coupling of Exit Duct to Inlet and Plenum	7
Pure Damping at the Plenum Exit	10
Energy Relationships	12
DESCRIPTION OF MODELS AND EXPERIMENTAL APPARATUS	15
EXPERIMENTAL RESULTS AND DISCUSSION	16
Modification of the Boundary Layer by Air Injection	16
Static Stability Investigation with Turbulent Boundary Layer	16
Static Stability Investigation with Laminar-Like Boundary Layer	19
Dynamic Stability Experiments	20
CONCLUSIONS	28
BIBLIOGRAPHY	29
TABLE I - MEASUREMENTS CONCERNING DYNAMIC STABILITY	30

Contrails

LIST OF ILLUSTRATIONS

Figure		Page
1	General View of Test Equipment	31
2	Suction Plenum with Cover Removed	31
3	Inside Wall View, Showing Suction Slot Without Splitters .	32
4	Inside Wall View, Showing Suction Slot With Splitters . .	32
5a	Diagram of Suction System	33
5b	Detail of Slot and Diffuser Geometry	34
5c,d,e,f	Devices Used to Investigate Alleviation of Static Instability	35
6	Splitter Plate Installation - Four Sections Open	36
7	Splitter Plate Installation - Two Sections Open	36
8	Effect of Boundary Layer Suction on Free-Stream Velocity and Boundary Layer Profile	37
9	Effect of Boundary Layer Profile on Static Stability (Two- Slot System)	38
10	Effect of Boundary Layer Profile on Pressure Recovered in Plenum (Four-Slot System)	39
11	Pressure Variations With Two-Slot System With Various Schemes to Alleviate Static Instability	40
12	Effect of Tunnel Velocity and Boundary Layer Shape on Pressure Recovered in Plenum	41
13	Maximum Available Pressure Calculated from Momentum of Boundary Layer	42
14	Effect of Splitter Plates on Pressure Recovered in Plenum	43
15	Effect of Plenum Volume on Pressure Recovered in Plenum .	44
16	Pressure Recovery in Diffuser	45
17a,b	Dynamic Pressure Variations in Suction System	46
17c,d	Dynamic Pressure Variations in Suction System	47
18a,b	Dynamic Pressure Variations in Suction System	48

Contrails

LIST OF SYMBOLS

a	speed of sound	ft/sec
A_e	cross-sectional area of exit duct	ft ²
A_s	cross-sectional area of inlet duct at entrance to the duct	ft ²
A, B	constants in solution of differential equation for velocity potential (see page 5)	ft ² /sec
b_e', b_s'	damping coefficients defined by Eqs. (38) and (39)	1/sec
c_{11}, c_{22}	damping parameters defined by Eq. (51)	lb sec/ft ⁵
f_s	$\omega_s/2\pi$	1/sec
H	shape parameter for boundary layer	$\equiv \frac{\delta^*}{\theta}$
H_s	total head of flow entering plenum chamber	lb/ft ²
H_1	total head of flow in duct	lb/ft ²
k	ω/a	1/ft
K	plenum chamber "spring constant." See Eq. (22)	lb/ft ⁷
l, l_e	length of exit duct	ft
l_s	length of entrance duct	ft
m_{11}	mass parameter for entrance duct	lb sec ² /ft ⁷
m_{22}	mass parameter for exit duct	lb sec ² /ft ⁷
p	oscillatory pressure of air in exit duct ($t=0$)	lb/ft ²
$P(x, t)$	$p e^{-i\omega t}$	lb/ft ²
p_0	value of p at entrance to exit duct ($x=0$)	lb/ft ²
p_l	value of p at end of exit duct ($x=l$)	lb/ft ²
P_0	tunnel static pressure	lb/ft ²
P_1	static pressure in duct	lb/ft ²
P	complex frequency	1/sec
q_s	volume rate of flow in inlet duct	ft ³ /sec
q_e	volume rate of flow in exit duct	ft ³ /sec

Contrails

LIST OF SYMBOLS (Continued)

q_{s_0}	time averaged flow rate in entrance duct	ft^3/sec
q_{e_0}	time averaged flow rate in exit duct	ft^3/sec
Q	suction flow rate divided by suction required to remove 1/4 of turbulent boundary layer	
t	time	sec
T	period of oscillation	sec
u	velocity of air in exit duct at time $t = 0$	ft/sec
$U(x, t)$	$u e^{-i\omega t}$	ft/sec
u_e, u_0	velocity of air at entrance to exit duct ($x = 0$)	ft/sec
u_l	velocity of air at end of exit duct ($x = l$)	ft/sec
U	nonuniform velocity of air in boundary layer	ft/sec
U_1	uniform velocity of air after mixing in duct	ft/sec
V	plenum volume	ft^3
x	position coordinate measured along axis of exit duct ($x = 0$ at plenum chamber)	ft
y	position coordinate measured perpendicular to tunnel wall	ft
Z, Z_e	acoustic impedance of exit duct	$\text{lb sec}/\text{ft}^3$
Z_e^R	real part of Z_e	$\text{lb sec}/\text{ft}^3$
Z_e^I	imaginary part of Z_e	$\text{lb sec}/\text{ft}^3$
α	acoustic impedance of flow metering device	$\text{lb sec}/\text{ft}^3$
δ	partial boundary layer depth from which flow is taken during suction	ft
δ^*	boundary layer displacement thickness (see page 16)	ft
ζ	effective displacement of air in a short exit duct, when such a duct is considered as an air spring	ft
ζ_s	dimensionless correction factor to account for inlet duct taper [see Eq. (21)]	

Contrails

LIST OF SYMBOLS (Continued)

θ	phase angle by which the plenum pressure leads the velocity in the exit pipe	degrees
θ	boundary layer momentum thickness (used on page 16)	
$\int_0^t \dot{V}_s$	volume of air which has entered plenum from exit duct at time t , due to oscillatory motion	ft^3
$\int_0^t \dot{V}_e$	volume of air which has left plenum through exit duct at time t , due to oscillatory motion	ft^3
$\bar{\xi}_s$	maximum value of ξ_s during oscillation	$\bar{\xi}_s = \xi_s e^{-i\omega t}$ ft^3
$\bar{\xi}_e$	maximum value of ξ_e during oscillation	$\bar{\xi}_e = \xi_e e^{-i\omega t}$ ft^3
ρ	density of air	slug/ ft^3
ϕ	velocity potential (exit duct) at time $t=0$ (as used on pages 4 and 5)	ft^2/sec
Φ	$\phi e^{-i\omega t}$ (as used on pages 4 and 5)	ft^2/sec
ϕ	phase angle by which entrance duct flow leads exit duct flow	degrees
ω	angular frequency	1/sec
ω_s, ω_1	uncoupled frequency of inlet duct	1/sec
ω_e, ω_2	uncoupled frequency of exit duct	1/sec

Contrails

INTRODUCTION

Aircraft induction systems which ingest air from a boundary layer often encounter flow instability. The most common cases of this kind of instability have occurred in engine air intakes, and the instability in such cases has usually been eliminated by diverting the boundary-layer air from the intake or by bleeding it off ahead of the intake. Recently, there has been renewed interest in the use of boundary layer suction systems to improve the maximum lift and the minimum drag of aircraft (Refs. 3, 4, 5, 6). For such systems, practically the entire mass of air being taken into the system is boundary-layer air, and careful attention to flow stability in such systems is necessary. The earliest theoretical study of flow instability in boundary layer inlets seems to have been that of Smith and Roberts (Refs. 5 and 8). They showed that for flow rates less than those necessary to suck the entire boundary layer, the total head of the air entering the system may have a positive increase with increase of volume flow. This system characteristic is known to be associated with flow instability in the phenomena of compressor surge (Ref. 7), supersonic diffuser "buzz", and twin duct instability of jet engine intakes (Ref. 9). In Reference 1, the stability of a boundary layer suction system was considered in greater detail, and it was shown that the criteria for instability depended not only on the characteristics of the inlet, but also on the characteristics of the entire duct system following the inlet.

In Reference 1, results were reported on tests conducted with a suction system taking turbulent boundary-layer air from the 16-inch wall of the C.A.L. 3 inch x 16 inch subsonic wind tunnel. When a single wide slot (13.75 in.) was employed, flow instability of both the static and dynamic types was encountered simultaneously. The static instability manifested itself in the form of a non-uniform flow across the inlet with greater than average inflow at one end and outflow at the other end. At the same time the system exhibited dynamic instability in the form of regular oscillations. By dividing the slot into four smaller sections, with splitter plates, the oscillations could be eliminated, but the static instability remained, as evidenced by the nonuniform distribution of flow among the four sections. Attempts were also made to investigate a system ingesting a laminar boundary layer on a model airfoil mounted in the same wind tunnel. No instability was, however, observed in the airfoil model system with either laminar boundary layer or turbulent boundary layer (induced by a trip wire on the airfoil). Two possible causes for the stability of the airfoil model system irrespective of boundary-layer profile were seen: first, the smaller scale of the slot and inlet might have produced higher losses than were encountered with the tunnel wall suction system and second, the decreased system volume might have been sufficient to make the system stable as indicated qualitatively by theory. The dynamic instrumentation of these tests was inadequate to allow any correlation of theory with experimental results, since the tests were only exploratory in nature, and were originally aimed primarily at the investigation of static instability.

The present program was aimed at amplifying the results obtained in Reference 1, and in particular at investigating the effect of boundary-layer profile on the flow instability. Also, effort was directed to obtaining sufficient data under oscillatory conditions to allow correlation of the results of dynamic theory with experiment. Since it did not appear convenient to ob-

Manuscript released by the authors in August 1955 for publication as a WADC Technical Report.

Contrails

tain a true laminar boundary layer on the wind tunnel wall, an artifice first developed by Wieghardt (Ref. 2) was employed to obtain a thick laminar-like boundary-layer profile. This involved bleeding air through a perforated sheet into the boundary layer ahead of the inlet slot. Measured velocity profiles showed that a practically linear velocity distribution through the boundary layer could be obtained in this way. Tests carried out with this laminar-like boundary layer showed no dynamic instability and very little evidence of static instability. These results correlated well with the theoretical stability criteria, since the laminar-like boundary layer had a substantially lower slope of the curve of inlet total head versus volume flow than the turbulent boundary layer. It was also found that the reduction of system volume necessary to make the system stable with turbulent boundary layer inflow was in good agreement with theoretical predictions. This also accounts for the observed stability of the airfoil model suction system with turbulent boundary layer reported in Reference 1. In order to carry out a quantitative comparison between theory and experiment for dynamic stability, it was necessary to carry out a more complete analysis of the exit duct (which consisted of a long pipe) than was given in Reference 1. This analysis, which is presented herein, takes account of acoustic wave propagation in the pipe and the losses in the venturi at the end of the pipe. An energy analysis for the oscillating system could then be carried out in which the input of energy from the inlet was balanced by the dissipation of energy in the exit duct. The measured amplitudes and phase angles for the flow in the inlet and exit ducts were in fair agreement with the analytical results.

It appears in general that the methods employed in this investigation may find wider application to many kinds of duct systems. In particular it is significant that, at least under the conditions of these tests, the inlet characteristics measured under nonoscillatory conditions could be applied under oscillatory conditions. On the other hand, the determination of the exit duct characteristics under oscillatory conditions from dynamic total and static pressure measurements also demonstrates the feasibility of measuring component dynamic characteristics, and with improved techniques of instrumentation and calibration may well offer accuracy comparable with the static measurements. The exit duct characteristics are then obtained in the form of an impedance (ratio of pressure to velocity at the entrance) versus frequency, and perhaps amplitude if the system were highly nonlinear. This then would completely define the dynamic characteristics of the system with respect to other elements to which it might be coupled, and would allow dynamic matching of ducts to inlets, plenum chambers, exhaust pumps, or even engines and other mechanical or aerodynamic components. Such an approach might, for instance, allow the surge characteristics of an inlet, duct system, and suction pump or engine to be computed from element tests long before a completed aircraft could be available for test.

Boundary-Layer Characteristics

In Reference 1, the total head recovery from a flow of air originating in the boundary layer was discussed on the basis of the total energy of the flow. Actually, due to mixing losses, the total energy of the flow is not a good index of the available total head. A better index is probably the total head which would be recovered from the nonuniform entering stream if mixing took place in a long duct of constant section. In such mixing the total momentum of the stream is constant. Thus, if the partial boundary layer depth from which the flow is taken is δ , the duct is assumed to be of dimension δ also. If U_1 denotes the uniform velocity after mixing and U denotes the nonuniform velocity before mixing, the equation of continuity gives

$$U_1 = \frac{1}{\delta} \int_0^{\delta} U dy$$

The momentum equation is

$$P_0 + \frac{1}{\delta} \int_0^{\delta} \rho U^2 dy = P_1 + \rho U_1^2$$

since the pressure P_0 is constant through the boundary layer. The total head after mixing is

$$H_1 = P_1 + \frac{1}{2} \rho U_1^2$$

On substituting from the energy and momentum equation for P_1 and U_1 , we have

$$H_1 - P_0 = \frac{1}{\delta} \int_0^{\delta} \rho U^2 dy - \frac{1}{2} \rho \left(\frac{1}{\delta} \right)^2 \left[\int_0^{\delta} U dy \right]^2$$

This result may be nondimensionalized by dividing by $\frac{1}{2} \rho U_0^2$, where U_0 is the stream velocity outside the boundary layer, to give

$$\frac{H_1 - P_0}{\frac{1}{2} \rho U_0^2} = \frac{2}{\delta} \int_0^{\delta} \left(\frac{U}{U_0} \right)^2 dy - \left(\frac{1}{\delta} \right)^2 \left[\int_0^{\delta} \left(\frac{U}{U_0} \right) dy \right]^2$$

It is seen that the total head given by this formula depends only on the boundary layer profile, U/U_0 . Actually, of course, there are additional losses in the inlet duct which reduce the recoverable total head below this value. For comparisons of streams of different profile, however, the value given by this formula should indicate generally the relative magnitudes involved. Calculated curves of $(H_1 - P_0) / \frac{1}{2} \rho U_0^2$ are given in Fig. 13 for typical turbulent and laminar-type velocity profiles encountered in the present investigation. It may be seen from this figure that the turbulent profile leads to considerably higher pressure recovery for a given volume flow than the laminar profile.

Contrails

Dynamic Characteristics of the Exit Duct

The analysis of the inlet and exit ducts given in Reference 1 was based on the assumption that these ducts were short enough relative to the acoustic wavelength of the oscillations which might occur so that the air in them might be considered to be moving in essentially incompressible flow. This led to a description of the plenum chamber plus inlet and exit ducts as a Helmholtz resonator with two necks. In many applications this will not be the case, particularly as regards the exit duct. It is therefore desirable to investigate the characteristics of a long pipe with an orifice or other device producing a loss of head at the end. This can be done by means of the usual equations of acoustics for flow in ducts. In the experiments to be discussed herein, the mean flow velocity in the duct was low enough so that the mean flow effects can be neglected except as they affect the head loss at the end. If this is not the case, the more general equations for unsteady one-dimensional compressible flow should be used. These are somewhat more complicated, but would not alter the fundamental method of analysis in any important way.

The one-dimensional equation for the velocity potential, ϕ , in a duct is given by (Ref. 11)

$$\frac{\partial^2 \phi}{\partial x^2} + k^2 \phi = 0 \quad (1)$$

where x is distance along the duct and $k = \omega/a$, ω being the frequency and a the velocity of sound. The oscillatory velocity, u , in the duct and the oscillatory pressure, p , in the duct are given by

$$u = -\frac{\partial \phi}{\partial x} \quad (2)$$

$$p = -i\omega\rho\phi \quad (3)$$

the oscillatory motions being described by

$$U(x,t) = u e^{-i\omega t} \quad (4)$$

and

$$P(x,t) = p e^{-i\omega t}$$

also

$$\Phi(x,t) = \phi e^{-i\omega t} \quad (5)$$

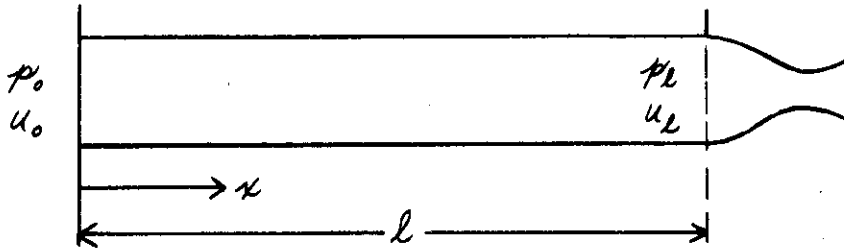
The duct to be analyzed will be assumed to have a prescribed pressure oscillation $P_0 = p_0 e^{-i\omega t}$ at the end $x=0$, and a flow metering device at

Contrails

$x=l$. The flow metering device can be described for small oscillations in terms of a linear relationship between the pressure p_l and velocity u_l , namely

$$p_l = \alpha u_l \quad (6)$$

The system is as shown below



The general solution to Eq. (1) is

$$\phi = A \cos kx + B \sin kx \quad (7)$$

where A and B are constants to be determined from the boundary conditions. From Eqs. (2) and (3)

$$p_0 = -i\omega\rho A \quad (8)$$

$$u_0 = -kB \quad (9)$$

$$p_l = -i\omega\rho [A \cos kl + B \sin kl] \quad (10)$$

$$u_l = kA \sin kl - kB \cos kl \quad (11)$$

The boundary condition at $x=l$ from Eq. (6) gives

$$A \left[-i\omega \cos kl - \frac{k\alpha}{\rho} \sin kl \right] = B \left[i\omega \sin kl - \frac{k\alpha}{\rho} \cos kl \right] .$$

Solving this for B gives

$$B = A \left[\frac{\left(\frac{k^2 \alpha^2}{\rho^2} - \omega^2 \right) \sin kl \cos kl + i \frac{\omega k \alpha}{\rho}}{\frac{k^2 \alpha^2}{\rho^2} \cos^2 kl + \omega^2 \sin^2 kl} \right] \quad (12)$$

Contrails

Substituting for A and B from Eqs. (8) and (9) gives

$$u_0 = \frac{p_0}{\rho a} \left[\frac{-i \left(\frac{k^2 \alpha^2}{\rho^2} - \omega^2 \right) \sin kl \cos kl + \frac{\omega k a}{\rho}}{\frac{k^2 \alpha^2}{\rho^2} \cos^2 kl + \omega^2 \sin^2 kl} \right] \quad (13)$$

A concept often used in acoustics is that of impedance, Z , which is simply the ratio of the oscillatory pressure to the oscillatory velocity at $x=0$. This is easily obtained as

$$Z = \frac{p_0}{u_0} = i \rho a \left[\frac{\left(\frac{k^2 \alpha^2}{\rho^2} - \omega^2 \right) \sin kl \cos kl - i \frac{\omega k a}{\rho}}{\frac{k^2 \alpha^2}{\rho^2} \sin^2 kl + \omega^2 \cos^2 kl} \right] \quad (14)$$

Insofar as the remainder of the system is concerned, Z gives all the necessary dynamical information about the exit duct. If the duct is relatively short so that $kl \ll 1$, and the damping is neglected ($\alpha \rightarrow 0$)

$$Z = -i \rho a k l = -i \rho \omega l \quad (15)$$

which describes the reaction of the duct as that of a mass of air of length l , being accelerated at a rate $-i\omega u$. This was the description of the exit duct used in Reference 1 except that a small damping loss α was included. If the damping is assumed finite but small so that $\frac{k^2 \alpha^2}{\rho^2}$ is negligible compared to ω^2 , there results from Eq. (14), for small kl ,

$$Z = -i \rho \omega l + \alpha \quad (16)$$

This is identical to what was actually used in Reference 1 for the exit duct characteristics.

If, on the other hand, $\frac{k a}{\rho}$ is very large compared to ω , the impedance becomes

$$Z = i \rho a \cot kl \quad (17)$$

which exactly corresponds to the well-known result for a tube with a closed end at $x=l$ (Ref. 11). This is reasonable since if there is enough resistance to flow at $x=l$, the tube should behave as if it were effectively closed. If kl is small at the same time, Eq. (17) reduces to

$$Z = i \frac{\rho a^2}{\omega l} = \frac{\rho a^2}{(-i\omega)l} \quad (18)$$

Contrails

which can be interpreted as meaning that the duct is acting as an air spring subjected to displacements ζ equal to $\frac{u}{-i\omega}$.

In general, the interpretation of the duct impedance is not so straightforward as for the cases discussed above, since the duct acts simultaneously as mass, air spring, and damper. The special case $kl = n\pi$ for integer n is of great interest, since $\sin kl$ is then zero and

$$Z = \alpha \quad (19)$$

This means that the duct is acting effectively as a pure damper without mass or spring action. This case is of importance in the experiments to be described herein, since it provided a simple means for measuring α under dynamic conditions without using an exit duct so short that flow measurements were questionable.

Coupling of Exit Duct to Inlet and Plenum

The equation of motion for the inlet and plenum system is taken directly from Reference 1 as

$$\frac{\rho l_s \zeta_s}{A_s} \frac{\partial q_s}{\partial t} - \frac{\partial H_s}{\partial q_s} q_s + K \int_0^t q_s dt - K \int_0^t q_e dt = 0 \quad (20)$$

where q_s is the rate of volume flow into the inlet, q_e is the rate of volume flow from the exit, l_s is the length of the inlet duct, A_s is the cross-sectional area of the inlet duct at the entrance to the duct, ρ is the air density, and $\frac{\partial H_s}{\partial q_s}$ is the slope of the curve of total head at the entrance to the plenum chamber versus volume flow rate. The factor ζ_s is a correction factor on the mass of air accelerated in the inlet duct to account for duct taper, and is given by

$$\zeta_s = \int_0^1 \frac{d(x/l_s)}{A/A_s} \quad (21)$$

K is the plenum chamber spring constant, and is given (Ref. 1) by

$$K = \frac{a^2 \rho}{V} \quad (22)$$

This equation is based on the assumption (which is usually valid for inlet ducts) that the duct is short compared to the acoustic wavelength of the oscillations, so that the flow in the duct is incompressible. The air in the duct is therefore considered to be accelerated without compression, and the simple equation of motion presented above results. It is worth noting that for a straight duct ($\zeta_s = 1$), the assumptions made are equivalent to those made in the derivation of Eq. (16) from Eq. (14) for a short duct, namely kl small.

Contrails

The results are, in fact, identical to Eq. (16) if $q = A_s u$ and $\frac{\partial u}{\partial t} = -i\omega u$ are substituted in Eq. (20), and if it is recognized that $\frac{\partial H_s}{\partial q_s}$ corresponds to α/A_s .

The treatment of the exit duct in Reference 1 was identical to the treatment of the inlet duct, and resulted in a similar equation of motion. The exit duct will here no longer be considered short so that a new equation for the exit duct must be obtained. The exit duct is subjected to the plenum chamber pressure, P_c , variation so that

$$\frac{P_c}{u_e} = Z_e \quad (23)$$

where u_e is the oscillatory flow velocity at the duct entrance. From Reference 1

$$P_c = K \int_0^t q_s dt - K \int_0^t q_e dt \quad (24)$$

Combining Eqs. (23) and (24)

$$Z_e u_e + K \int_0^t q_e dt - K \int_0^t q_s dt = 0 \quad (25)$$

Let

$$\left. \begin{aligned} \bar{\xi}_s &= \int_0^t q_s dt = \xi_s e^{-i\omega t} \\ \text{and} \\ \bar{\xi}_e &= \int_0^t q_e dt = \xi_e e^{-i\omega t} \end{aligned} \right\} \quad (26)$$

Then

$$A_e u_e = q_e = \frac{\partial \bar{\xi}_e}{\partial t} = -i\omega \xi_e e^{-i\omega t} \quad (27)$$

The equation of motion is

$$-i\omega \frac{Z_e}{A_e} \xi_e + K \xi_e - K \xi_s = 0 \quad (28)$$

In order to use the simple form of the impedance concept, this equation had to be derived on the basis of harmonic motion. This is not a serious limitation since in stability investigations the margin between positively damped and negatively damped motion is always characterized by harmonic motion. Actually, in the case of lightly damped motion it is often permissible to make the assumption that Z_e is applicable and is a function only of the frequency of the motion and not of its rate of growth or decay in that case, the approx-

Contrails

imate equation of motion is

$$\left(\frac{-Z_e^I}{\omega A_e} \right) \frac{\partial^2 \xi_e}{\partial t^2} + \frac{Z_e^{(R)}}{A_e} \frac{\partial \xi_e}{\partial t} + K \xi_e - K \xi_s = 0 \quad (29)$$

where Z_e has been split into real and imaginary parts to give

$$Z_e = Z_e^R + i Z_e^I \quad (30)$$

If Z_e for small kl_e is substituted from Eq. (16), the above equation becomes identical with that derived for the exit mass in Reference 1.

For calculation of the undamped natural frequencies of the system, the motion to be considered is of course harmonic, and the use of the impedance formula is exactly correct if the oscillation amplitude is small enough. The impedance is then necessarily pure imaginary. The equations for undamped natural frequency which replace the Helmholtz resonator formula Eq. (32) of Ref. 1 are

$$\left. \begin{aligned} \frac{\rho l_s \xi_s}{A_s} \frac{\partial^2 \xi_s}{\partial t^2} + K \xi_s - K \xi_e &= 0 \\ \left(\frac{-Z_e^I}{\omega A_e} \right) \frac{\partial^2 \xi_e}{\partial t^2} + K \xi_e - K \xi_s &= 0 \end{aligned} \right\} \quad (31)$$

Z_e^I is obtained from Eq. (14) as

$$Z_e^I = \rho a \left[\frac{\left(\frac{\alpha^2}{a^2 \rho^2} - 1 \right) \sin kl_e \cos kl_e}{\frac{\alpha^2}{a^2 \rho^2} \sin^2 kl_e + \cos^2 kl_e} \right] \quad (32)$$

Since this result depends on the pressure loss coefficient, α , at the end of the exit duct in an essential way, it may appear questionable whether the "undamped" frequency has any real meaning in this case. It can, however, easily be realized that while the magnitude of the loss coefficient almost completely determines the behavior of the exit duct, it need not necessarily provide a large dissipation of energy of the system as a whole to be important. The undamped natural frequency results from the solution of

$$\left. \begin{aligned} \left(-\frac{\rho l_s \xi_s}{A_s} \omega^2 + K \right) \xi_s - K \xi_e &= 0 \\ \left(\frac{Z_e^I}{A_e} \omega + K \right) \xi_e - K \xi_s &= 0 \end{aligned} \right\} \quad (33)$$

The determinant of these equations must be zero for undamped oscillation, and this leads finally to

$$\left(\omega^2 - \omega_s^2 \right) + \frac{a A_e}{V} \left(\frac{\rho a}{Z_e^I} \right) \omega = 0 \quad (34)$$

Contrails

where

$$\omega_s^2 = \frac{KA_s}{\rho l_s \zeta_s} \quad (35)$$

and
$$K = \frac{a^2 \rho}{V} \quad (36)$$

have been used to simplify the results.

Pure Damping at the Plenum Exit

In the case where the exit duct imposes only damping resistance on the plenum chamber (for instance, when $kl_e \approx \pi$, as discussed above), the equations of motion assume a simple form, since the exit impedance is given by $Z = \alpha$ [See Eq. (19)]. The equations of motion are

$$\left. \begin{aligned} \frac{\rho l_s \zeta_s}{A_s} \frac{\partial^2 \xi_s}{\partial t^2} - \frac{\partial H_s}{\partial q_s} \frac{\partial \xi_s}{\partial t} + k \xi_s - k \xi_e &= 0 \\ \frac{\partial p_e}{\partial q_e} \frac{\partial \xi_e}{\partial t} + k \xi_e - k \xi_s &= 0 \end{aligned} \right\} \quad (37)$$

where $\frac{\partial p_e}{\partial q_e}$ has been substituted for $\frac{\alpha}{A_s}$

Let

$$b_s = - \frac{\partial H_s}{\partial q_s} \frac{A_s}{\rho l_s \zeta_s} \quad (38)$$

$$b_e' = \frac{\partial p_e}{\partial q_e} \frac{A_s}{\rho l_s \zeta_s} \quad (39)$$

$$\omega_s^2 = \frac{k A_s}{\rho l_s \zeta_s} \quad (40)$$

Also substitute the solutions

$$\left. \begin{aligned} \bar{\xi}_s &= \xi_s e^{pt} \\ \bar{\xi}_e &= \xi_e e^{pt} \end{aligned} \right\} \quad (41)$$

to give

$$\left. \begin{aligned} (p^2 + b_s p + \omega_s^2) \xi_s - \omega_s^2 \xi_e &= 0 \\ -\omega_s^2 \xi_s + (b_e' p + \omega_s^2) \xi_e &= 0 \end{aligned} \right\} \quad (42)$$

Setting the determinant of this system equal to zero leads to

$$p^2 + \left(\frac{\omega_s^2 + b_s b_e'}{b_e'} \right) p + \omega_s^2 \left(\frac{b_s + b_e'}{b_e'} \right) = 0 \quad (43)$$

Contrails

of which the solution is

$$p = - \left[\frac{\omega_s^2 + b_s b_e'}{2 b_e'} \right] \pm \sqrt{\left[\frac{\omega_s^2 + b_s b_e'}{2 b_e'} \right]^2 - \omega_s^2 \left(\frac{b_s + b_e'}{b_e'} \right)} \quad (44)$$

For oscillation, the quantity under the square root sign must be negative, and for instability, the amplitude must increase in time, so that the real part of p must be positive. Thus the condition for instability is that

$$\omega_s^2 + b_s b_e' < 0 \quad (45)$$

This is equivalent to the more general stability criterion given in Reference 1 when the exit duct mass and stiffness terms may be neglected. The criterion for instability may be restated as

$$\frac{a^2}{V} - \frac{\partial H_s}{\partial q_s} \frac{\partial p_e}{\partial q_e} \frac{A_s}{\rho^2 l_s \zeta_s} < 0 \quad (46)$$

The frequency of the motion is given by

$$\omega = \sqrt{\omega_s^2 - \frac{1}{4} \left(\frac{\omega_s^2}{b_e'} - \frac{b_s}{2} \right)^2} \quad (47)$$

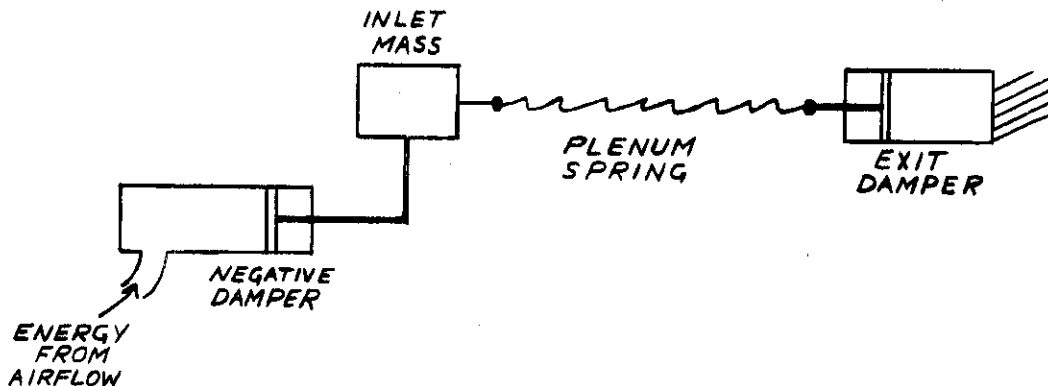
The frequency formula is interesting in that the damping plays an important role. For instance, if $b_s = 0$ (no inlet negative damping)

$$\omega = \sqrt{\omega_s^2 - \frac{1}{4} \left(\frac{\omega_s^2}{b_e} \right)^2} \quad (48)$$

and no oscillation will occur unless

$$b_e > \frac{\omega_s}{2} \quad (49)$$

This is the critical value of damping coefficient in the usual sense. A system in which a single mass is restrained by a spring and damper would not oscillate if the damping coefficient were greater than this quantity. On the contrary, the present system will not oscillate unless the damping coefficient is greater than this quantity. The mechanical analogue of the present system is shown below



Contrails

It is obvious in this system that with low enough exit damping the spring will be relatively unrestrained and no oscillation will occur.

Energy Relationships

If it is assumed that the stiffness terms in the equations of motion are linear in displacement, a simple relation between the amplitude of the motion and the damping coefficients may be obtained. This was done in Reference 1 for the single degree of freedom system consisting of the inlet and plenum chamber only. For the two degree of freedom system consisting of inlet and exit ducts, the equations of motion may be written as

$$\left. \begin{aligned} m_{11} \frac{d^2 \xi_s}{dt^2} + c_{11} \frac{d \xi_s}{dt} + K \xi_s - K \xi_e &= 0 \\ m_{22} \frac{d^2 \xi_e}{dt^2} + c_{22} \frac{d \xi_e}{dt} + K \xi_e - K \xi_s &= 0 \end{aligned} \right\} \quad (50)$$

where for convenience

$$\left. \begin{aligned} m_{11} &= \frac{\rho l_s \xi_s}{A_s} \\ m_{22} &= \frac{\rho l_e \xi_e}{A_e} \\ c_{11} &= -\frac{\partial H_s}{\partial q_s} \\ c_{22} &= \frac{\partial p_e}{\partial q_e} \end{aligned} \right\} \quad (51)$$

are used.

Multiplying the first equation by $\frac{d \xi_s}{dt}$ and the second by $\frac{d \xi_e}{dt}$ and integrating over the period T gives

$$\begin{aligned} &\int_0^T m_{11} \frac{d \xi_s}{dt} \frac{d^2 \xi_s}{dt^2} dt + \int_0^T m_{22} \frac{d \xi_e}{dt} \frac{d^2 \xi_e}{dt^2} dt \\ &+ \int_0^T K \left[\xi_s \frac{d \xi_s}{dt} + \xi_e \frac{d \xi_e}{dt} - \xi_s \frac{d \xi_e}{dt} - \xi_e \frac{d \xi_s}{dt} \right] dt \\ &+ \int_0^T c_{11} \left(\frac{d \xi_s}{dt} \right)^2 dt + \int_0^T c_{22} \left(\frac{d \xi_e}{dt} \right)^2 dt = 0. \end{aligned}$$

The first two integrals are exact differentials and may be integrated so that

$$\left[\frac{m_{11}}{2} \left(\frac{d\xi_s}{dt} \right)^2 + \frac{m_{22}}{2} \left(\frac{d\xi_e}{dt} \right)^2 \right] \Big|_0^T$$

$$+ K \left[\frac{\xi_s^2}{2} - \xi_s \xi_e + \frac{\xi_e^2}{2} \right] \Big|_0^T$$

$$+ \int_0^T \nu_{11} \left(\frac{d\xi_s}{dt} \right)^2 dt + \int_0^T \nu_{22} \left(\frac{d\xi_e}{dt} \right)^2 dt = 0 .$$

For periodic motions, the values of ξ and $\frac{d\xi}{dt}$ are the same at 0 and T so that

$$- \int_0^T \nu_{11} \left(\frac{d\xi_s}{dt} \right)^2 dt = \int_0^T \nu_{22} \left(\frac{d\xi_e}{dt} \right)^2 dt = 0 .$$

At the stability margin for ν_{11} and ν_{22} constant

$$\xi_s = |\xi_s| \sin \omega t$$

$$\xi_e = |\xi_e| \sin(\omega t + \phi)$$

where ϕ is the phase angle between ξ_e and ξ_s . Thus if ν_{11} and ν_{22} are constant

$$- \nu_{11} |\xi_s|^2 \int_0^T \omega^2 \cos^2 \omega t dt$$

$$= \nu_{22} |\xi_e|^2 \int_0^T \omega^2 \cos^2(\omega t + \phi) dt .$$

The two integrals give the same result so that

$$- \nu_{11} |\xi_s|^2 = \nu_{22} |\xi_e|^2$$

$$\text{or } \frac{|\xi_s|}{|\xi_e|} = + \sqrt{\frac{\nu_{22}}{\nu_{11}}} = \sqrt{\frac{\partial p_e / \partial q_e}{\partial H_s / \partial q_s}} \quad (52)$$

If the damping is not constant the differential equation is nonlinear and the terms $\nu_{11} \frac{d\xi_s}{dt}$ and $\nu_{22} \frac{d\xi_e}{dt}$ must be replaced by $H_s(q_s) - H_s(q_{s_0})$ and $p_e(q_e) - p_e(q_{e_0})$ respectively. Here q_{s_0} and q_{e_0} are the flow rates corresponding to the nonoscillatory flow. The requirement for periodic motion is then

$$\int_0^T [H_s(q_s) - H_s(q_{s_0})] q_s dt$$

$$= \int_0^T [p_e(q_e) - p_e(q_{e_0})] q_e dt .$$

Controls

Returning to Eqs. (50), it is possible to derive an expression for the frequency of any periodic motion of the system in terms of the relative amplitudes and phase angles. To do this simply, however, it is necessary to assume that the damping term is linear and that the motion is sinusoidal. The first of Eqs. (50) is multiplied by ξ_s and the second by ξ_e . Adding the resulting equations and integrating over a period, there results

$$\int_0^T m_{11} \frac{d^2 \xi_s}{dt^2} \xi_s dt + \int_0^T m_{22} \frac{d^2 \xi_e}{dt^2} \xi_e dt + \int_0^T c_{11} \frac{d \xi_s}{dt} \xi_s dt + \int_0^T c_{22} \frac{d \xi_e}{dt} \xi_e dt + \int_0^T K \xi_s^2 dt - 2 \int_0^T K \xi_s \xi_e dt + \int_0^T K \xi_e^2 dt = 0$$

The terms in c_{11} and c_{22} are exact differentials and with an integration over a cycle are identically zero. To evaluate the remaining integrals, the substitutions

$$\xi_s = |\xi_s| \sin \omega t$$

$$\xi_e = |\xi_e| \sin(\omega t - \phi)$$

are made as in the previous discussion. This leads to

$$-\frac{\omega^2}{\omega_1^2} |\xi_s|^2 + |\xi_s|^2 - 2 |\xi_s| |\xi_e| \cos \phi - \frac{\omega_1^2}{\omega_2^2} \frac{\omega^2}{\omega_1^2} |\xi_e|^2 + |\xi_e|^2 = 0$$

where the substitutions

$$\omega_1^2 = \frac{K}{m_{11}}$$

$$\omega_2^2 = \frac{K}{m_{22}}$$

have been made. These represent the "uncoupled" or independent frequencies of the inlet duct plus plenum chamber and the exit duct plus plenum chamber, respectively. Finally,

$$\frac{\omega^2}{\omega_1^2} = \frac{1 - 2 \frac{|\xi_e|}{|\xi_s|} \cos \phi + \frac{|\xi_e|^2}{|\xi_s|^2}}{1 + \frac{\omega_1^2}{\omega_2^2} \frac{|\xi_e|^2}{|\xi_s|^2}} \quad (53)$$

This provides a relationship between the frequency of the coupled system and the frequencies of the component parts of the system in terms of the relative amplitudes and phases of the motion in the two components.

DESCRIPTION OF MODELS AND EXPERIMENTAL APPARATUS

The experimental work in this program was performed in the Cornell Aeronautical Laboratory 3 in. x 16 in. subsonic induction tunnel. This tunnel is powered by the 600 hp Nash pumps used for pressurization of the C.A.L. 8-1/2 ft x 12 ft Variable Density Tunnel. The test section pressure distribution for this tunnel, for the tunnel empty condition, is given in Reference 12.

A slot 14 in. wide was cut in the tunnel wall for the removal of the boundary-layer air. This slot was followed by a 12° diffuser making an angle of 30° with the direction of tunnel flow and emptying into a large plenum chamber. The plenum chamber was connected to a 40 hp Kinney positive displacement vacuum pump by a long 4 in. diameter pipe. The pipe was equipped with a venturi tube for measuring the suction rate and a large gate valve to control the suction.

Upstream of the suction slot, a section of the tunnel wall was replaced by a 15 in. x 16 in. porous sheet. Air was blown through this sheet in those experiments where a modified boundary layer was desired. The sheet was covered by a plenum chamber attached to the compressed air lines. Figure 5a shows a cutaway view of this apparatus.

The diffuser was designed to provide good pressure recovery and to be easily adjustable in width. Three downstream sections of the diffuser were provided so that by changing this section, slot widths of 0.5, 1, and 1.3 in. could be obtained. The diffuser angle remained 12° for all three slot widths. It was necessary to curve the diffuser in order to avoid the piping supplying the jet drives of the tunnel.

Total head tubes, reverse total head tubes, and static taps were installed at four points across the diffuser to give pressure and velocity measurements. These tubes can be seen in Fig. 3. This picture also shows the movable boundary layer rake that was used to obtain boundary-layer-profile data. Several static taps were provided in the tunnel wall immediately ahead of the slot, and two taps were installed in the suction plenum. Measurements in the exit pipe were obtained from static and total head probes 14 in. from the plenum.

The oscillating pressures in the system were measured with two Statham dynamic pressure pickups recording on a two-pen Brush oscillographer. The two pickups were vented to various points in the system in such a way that phase relations between any two points could be obtained. These pressure transducers can be seen in the general view of test equipment, Fig. 1.

In some of the tests it was desirable to divide the suction slot into separate sections, all entering the common plenum. For this purpose a set of three splitter plates, held in place by spacing rods, was inserted in the diffuser. A cutaway of this installation is shown in Fig. 6. The splitter plates are also visible in Figs. 2 and 4. Figure 7 shows the arrangement which provided a two-slot system. The top and bottom slots of the diffuser were closed by blocks, these blocks fitting flush with the tunnel wall. All these changes could be made by removing the plenum cover plate, as indicated in Fig. 2, and/or by removing the opposite tunnel wall, as shown in Figs. 3 and 4.

Modification of the Boundary Layer by Air Injection

The first experimental work in this program was concerned with modifying the normal turbulent boundary layer in the wind tunnel to obtain a velocity gradient less severe than that in the turbulent layer. A true laminar boundary layer could be obtained in the tunnel with a small airfoil model and with low tunnel speed. In this case the boundary layer would be very thin (~ 0.05 in.) and the suction slot width would necessarily be of this magnitude. It was suspected (Ref. 1), however, that stability results from small-scale suction models (with the attendant high losses) and from low tunnel speeds (with low dynamic head). Since both of these effects are stabilizing, a method was employed to modify the boundary layer by introducing air through the tunnel wall. The general method is described by Wieghardt in Reference 2. The main difference in the experimental arrangement is that in these experiments the air was introduced through a perforated sheet in a flat portion of the tunnel wall, while Wieghardt used a model of a wing nose, formed with perforated sheet. The results, however, were substantially the same. The boundary-layer profile downstream of the perforated sheet showed a thick laminar-like profile. Figure 8 shows a comparison of the normal turbulent boundary layer and the laminar-like layer obtained with blowing. These measurements were taken about 1 in. downstream of the perforated sheet (see Fig. 2) and directly in front of the suction slot. At four to five inches downstream, the boundary layer began to return to the turbulent profile, and at 10 in. the effect of blowing had largely disappeared.

The porous tunnel wall used in these experiments was Erdle IT 20% open perforated brass sheet (Erdle Perforating Company, Rochester, New York). The sheet was fitted to span the entire width of the tunnel (16 in.), and was 15 in. long. To obtain the desired boundary layer, it was necessary to go to high blowing rates (about $10 \text{ ft}^3/\text{sec}$), although it is possible that the 15 in. length of sheet could have been reduced to half that value and the blowing rate decreased proportionally. The sheet is shown schematically in Fig. 5 and appears in the pictures in Figs. 2 and 3.

In referring to the turbulent and laminar-like boundary layers, the boundary-layer shape parameter H has been used as an index, where H is defined by $H = \delta^*/\theta$. δ^* , the boundary-layer displacement thickness, and θ , the boundary-layer momentum thickness, are defined by

$$\delta^* = \int_0^{\delta} \left(1 - \frac{u}{u_0}\right) dy \qquad \theta = \int_0^{\delta} \left(1 - \frac{u}{u_0}\right) \frac{u}{u_0} dy$$

where δ is the thickness of the boundary layer. The shape parameter H was calculated from the measured boundary-layer profile.

Static Stability Investigation with Turbulent Boundary Layer

When suction was applied to the slot-diffuser system shown in Fig. 5, static instability was observed in the form of unequal flow rates at points across the span of the diffuser. The instability observed was the same as that described in Reference 1, including negative flow in some parts of the diffuser (flow into the tunnel) at the lower suction rates.

Controls

Inserting splitter vanes in the diffuser, so that it is divided into separate sections, accents this instability by cutting down on cross-flow effects. The resulting suction flow is characterized by large velocities in one section of the diffuser with small negative flow in the other sections. If the suction rate is increased, a point is reached where the flow pattern suddenly readjusts, and roughly equal flows are obtained in two sections, with small negative flow in the rest. Further increase in suction increases the flow in these two sections, until finally there is another readjustment, and a third slot becomes operative. This pattern repeats until all slots are ingesting roughly equal amounts of flow.

The experimental arrangement for studying this phenomenon is illustrated in Fig. 4. Four slots were used, and later, to study means of alleviating the instability, a two-slot system was employed (Fig. 5). The instability discussed above is illustrated for the two-slot system in Fig. 9.

With the four-slot system, velocity measurements were made in the diffuser sections to determine the separate flow rates and pressure recovery in the plenum was measured as a function of total flow rate. Total head tubes were available for flow measurement in both directions in the diffuser.

Since the tunnel wall suction affected the tunnel velocity (and therefore the measured pressures), all pressures were referred to tunnel static pressure. These effects are illustrated in Fig. 14, where plenum pressure and tunnel static pressures are plotted relative to free stream. The difference of the two curves is plotted at the top of the figure, showing the change in plenum pressure without the tunnel velocity involved ^{1/}. This curve shows that the pressure recovery is higher with the splitter vanes inserted than without, probably because of their "straightener" effect on the diffuser flow.

In Fig. 10 (and in several other graphs) the zero net flow stability condition is shown to correspond to considerable recovered pressure in the plenum. In this particular case there is a large positive flow in one of the diffuser slots and small negative flow in the other three sections. This is the type of result that would be expected according to the discussion of a two-slot system, given in Reference 1. Unfortunately, there is an error in the figure on page 8 of Reference 1, since the addition of curves IV and V should result in a curve VII which indicates a positive pressure recovery for zero net flow ^q. However, the accompanying discussion in Reference 1 is correct, and since it is rather lengthy it will not be repeated here. For the four-slot system, the three slots with negative flow can be combined and represented by curve IV. The single slot with positive flow can be represented by curve V. The resultant flow yields a pressure recovery in the plenum of 12% of the dynamic head available in the tunnel and zero net suction. For increased suction the velocity in the single slot continues to increase, until a suction rate of

^{1/} This change in tunnel velocity with suction rate corresponds to the additional power supplied to the tunnel by the suction apparatus, and keeps the flow through the tunnel ejector jets essentially constant. Since tunnel flow at 200 ft/sec is 67 ft³/sec, and the maximum suction rate was 7 ft³/sec, the maximum velocity increase was about 10% (20 ft/sec). The effect is shown graphically in Fig. 8.

2.7 ft³/sec is reached. This is sufficient suction to remove twice the boundary layer immediately ahead of the operative slot. The flow rate as measured in the diffusers, however, shows an inflow of 4.5 ft³/sec in the operative slot, and an outward flow of 0.6 ft³/sec in each of the other three. Thus this slot operates alone until it draws three times the available boundary layer from the stream. The corresponding plenum pressure recovery is indicated by the dotted line in Fig. 10.

A small increase in suction rate now rearranges the flow, so that diffuser sections #2 and 3 divide the incoming flow, and negative flow remains in the other two sections. There is a large corresponding increase in plenum pressure when this occurs. From the curves of page 8, Reference 1, it is not surprising that such a discontinuous jump in plenum pressure can occur, but it is not consistent with the fact that such higher pressures were not measured with only one section drawing. This secondary increase to higher pressures also occurs with the two-slot system, and seems to indicate that the pressure recovered from each diffuser section of a multiple-slot system depends to some extent on factors other than the net flow in the particular section.

The results of the two-slot system, shown in Fig. 9, offer an excellent comparison with the theory discussed in Reference 1 for a two-slot system. For example, the zero net flow condition corresponds to a finite pressure recovery in the plenum, as discussed in Reference 1 and above. Comparison of Fig. 9 (solid line) with the figure on page 8 of Reference 1, shows that as suction increases in one of the two slots, the plenum pressure also increases. Further increase in net suction decreases the magnitude of the negative flow in slot "C" of Fig. 9, with an attendant decrease in plenum pressure. This corresponds to curve VII(b) of Reference 1, page 8. Still greater net suction causes unequal inflow in the two sections, as indicated by curve VII(a). It is interesting to notice in Fig. 9 that the two sections have interchanged roles at this point, section C ingesting the major fraction of the air. This feature is observed as a discontinuous change, and indicates the geometrically identical nature of the two slots so that a perturbation can interchange their roles in the instability. An increase in suction beyond this point causes equal inflow in both slots, and finally a pressure decrease corresponding to curve VI. The two-slot system described above was investigated with the 0.5 in. slot width. For the four-slot system, both a 0.5 in. and 1.0 in. slot width were used, but the results in the two cases were the same. The graphs of Figs. 10 and 14 refer to the 0.5 in. slot.

Several modifications of the two-slot system were made in an attempt to remove the static instability. In the first attempt, a one-inch-diameter tube was connected between the two operative sections of the diffuser, since a static pressure difference existed between the two sections under conditions of unequal flow rate. This interconnection is illustrated in Fig. 5c, and had been suggested in the initial proposal of this work. There was, however, no measurable effect on the static instability. It was then thought that a direct diversion of a part of the flow would be possible, and accordingly two half-inch flow diverters were installed between two adjacent slots. This arrangement is shown in Fig. 5e, and was similarly ineffective in stabilizing the system. With the idea that the 1/2 in. diverters were too small to transfer an appreciable portion of the flow, a one-inch diverter was installed

Continued

(Fig. 5d), reaching one-third of the distance across the operative section. This still had no effect on the measured flow pattern. In a final attempt at changing the unstable flow, a 40% open perforated sheet was installed in place of the solid wall separating the two sections. The configuration still behaved exactly as a two-slot system. The pressure recovered in the plenum chamber with these arrangements is shown in Fig. 11. The two-maxima curve, characteristic of the two-slot system, prevails in all cases.

Static Stability Investigation with Laminar-Like Boundary Layer

The injection of air through a porous wall of the tunnel results in a laminar-like boundary-layer profile at the suction slot, as discussed previously in this section. The dynamic head available from this air for a given increase in flow rate is less than that for the turbulent boundary. This is discussed in the section on Boundary-Layer Characteristics and is illustrated in Fig. 13. Since this fact seems to present a method of attacking the static instability, each configuration that showed poor velocity distribution in the suction diffuser was tested with this laminar-like layer. The tests were made at the same tunnel speeds as with the turbulent boundary layer, and with the same range of suction rates. The result in each case was a marked trend toward uniform spanwise flow distribution, as would be expected from Fig. 13. The effect of the laminar layer on the pressure recovered in the plenum is illustrated in Figs. 9, 10, 12, 14, and 15. The clearest experimental comparison can probably be obtained with the two-slot system, and is illustrated in Fig. 9. In this figure the relative airflows in the two diffuser sections (B and C) are shown in insets for various suction rates and for both turbulent and laminar-like boundary layers. In the turbulent case, the two sections do not remove air at the same rate unless the total amount removed exceeds about twice the air available in the boundary layer ahead of the slots (four units of suction). With the laminar-like layer the plenum has reached its maximum pressure at 1.6 units of suction, and the flow rates in the two slots have become equal. With further increase in suction the diffuser losses cause a rapid decrease in plenum pressure. Thus one can say that static stability is obtained with considerably lower suction rate with the laminar-like boundary layer, since the destabilizing effect of the large dynamic head is not present.

This same general effect is obtained with the other models, such as the four-slot system shown in Fig. 10. This figure shows the discontinuous changes in section flow rate that can occur with the turbulent boundary layer. Thus a flow rate of two units can be obtained either with large positive flow in one slot and small negative flow in three slots, or with positive flow in two slots and small negative flow in two slots. With the laminar-like boundary layer this static instability is much less pronounced and, at a suction rate of two units, three diffuser sections are operative. The diffusers without dividing splitters show a more uniform spanwise velocity with laminar-like boundary layers, as well as being dynamically stable. This static stability was reported in Reference 1 for experiments with an airfoil model with laminar flow, but in that case other stabilizing effects (such as small suction slot with high losses) were suspected of being primarily responsible for the static stability. These experiments show that the laminar-like layer is, of itself, capable of

increasing static stability. In cases of static instability with the laminar-like boundary layer, profile measurements were made in front of each of the separate sections. These profiles were found to be essentially the same, independent of whether or not the particular duct section was operative.

Dynamic Stability Experiments

When boundary-layer air was removed from the tunnel wall through a single-slot diffuser, dynamic instability was observed. The instability was indicated by regular pressure fluctuations in the plenum and in the entrance and exit ducts. These variations in pressure were recorded with two Statham dynamic pressure pickups connected to a two-pen Brush oscillograph. The pressure pickup points are indicated in Fig. 5a, including the tunnel static pressure, diffuser total and static pressures, plenum pressure, and exit pipe total and static pressures. The various measurements were made separately, using the second pen to record a reference pressure in the system (usually plenum pressure). In this way the phase relations of the various points in the system could be compared. Some of the oscillograph traces are shown in Figs. 17 and 18. Figures 17a, 18a, and 18b represent a dynamically unstable system. It was noted that the static instability was present at the same time in the form of nonuniform suction across the entrance slot.

Since the resonant frequency of the inlet-plenum system was calculated as $f_s = 25.8$ cycles/sec, care was taken to keep the pipe length away from $\lambda/4 = 10.6$ ft., where λ is the wavelength of the acoustic oscillations in the pipe. A total length to the venturi throat = 13 ft was used.

Preliminary experiments with laminar-like boundary layers showed that the best profiles obtained were of the order of 1.5 in. thick. In deciding on the width of suction slot to use, this figure was used as an upper limit. The slot sizes chosen were 0.5 in., 1.0 in., and 1.3 in. They were obtained by inserting different size blocks to form the aft end of the suction diffuser (see Fig. 5b). In this way the 6° half angle of the diffuser was preserved for the three slots, but the ratio of outlet to inlet area of the diffuser changed from 8.0 for the 0.5 in. slot to 3.0 for the 1.3 in. slot.

Dynamic instability was observed in the tests with the small slot (0.5 in.), with tunnel velocity of 200 ft/sec and with turbulent boundary layer. These experimental measurements are listed in Table I, lines 1 through 5. The other lines in the table represent tests where the flow was dynamically stable, or very nearly so. Column 3 gives the suction rate, measured, as in the graphs, in terms of the flow rate to remove 1/4 of the total boundary layer. This unit of measure was found convenient in describing the experiments where the slot was divided into four equal sections, and was preserved throughout the report. This unit corresponds to a suction rate of 1.25 ft³/sec for a tunnel speed of 200 ft/sec.

Column 4 lists the behavior of the system as regard dynamic stability. In cases where the oscillation was transitory, the column is marked "some oscillation." In these cases it was not possible to make quantitative measurements on other than the frequency because of the irregularity of the pressure variations. A typical Brush recording for line 8 is shown in Fig. 17b.

Column 5 lists the value of $|\xi_s - \xi_e|$ obtained from measurement of the amplitude of the plenum pressure, and use of formula (24)

$$\Delta P_c = K (\xi_s - \xi_e) \quad (54)$$

The values of ξ_s and ξ_e are proportional to the maximum oscillatory quantities of flow in the inlet and exit ducts respectively.

Column 6 contains the value of $|\xi_e^*|$ calculated from dynamic measurements in the exit pipe. The error limits are the mean deviation for about ten separate readings. $|\xi_e|$ can be calculated from the relation $\xi_e = -\frac{1}{i\omega} \dot{\xi}_e$ and column 7 gives the ratio $\frac{|\xi_s - \xi_e|}{|\xi_e|}$.

Column 8 gives the absolute value of the impedance of the exit pipe in units of ρa . These values were calculated directly from dynamic measurements of plenum pressure and exit pipe velocity. Column 9 gives the phase angle between the quantities, obtained from the same measurements. This angle θ is defined as the angle by which the plenum pressure leads the velocity in the pipe. The frequency of the oscillation is given in column 10. Column 11 gives the average slope of the plenum pressure vs. flow rate curve, $\frac{\partial H}{\partial q}$. This is obtained from the static measurements for stable flow, and is given in units of $\text{lb/ft}^2/\text{ft}^3/\text{sec}$.

In Table I, columns 4, 5, 6, 9, 10, and 11 are the results of independent measurements. In particular, columns 5 through 9 are obtained from measurements of the pressures (static and total) in the exit pipe and the pressure in the plenum chamber, including the relative phases. The first two of these define the exit pipe velocity $\dot{\xi}_e$ listed in column 6. The measured phase angle between this and the plenum pressure is column 9, and the magnitude of the plenum pressure variation gives column 5. Columns 7 and 8 can then be obtained from 5 and 6. In the discussion that follows, these quantities are calculated theoretically, using as a basis the measured value of $|Z|$ and f from line 2. In a series of tests having to do with nonoscillating systems, the test reported in Table I is the one which should be most likely to oscillate. The other tests in each series were, of course, also stable. Tests where stabilizing effects were introduced with originally stable configurations, such as the 1.0 in. slot with laminar-like boundary layer and/or small plenum volume are not listed in the table, since the flow was dynamically stable in these cases and no new dynamic information was obtained.

Using Eq. (14) in the theoretical development one can obtain an expression for the magnitude of the impedance of the exit pipe in terms of the exit loss coefficient α , the frequency $\omega = 2\pi f$, and the pipe length l . This relation is

$$\left| \frac{Z}{\rho a} \right| = \frac{\sqrt{\left(\frac{\alpha}{\rho a}\right)^2 + \left(1 - \frac{\alpha^2}{a^2 \rho^2}\right)^2} \cos kl \sin kl}{\left(\frac{\alpha}{\rho a}\right)^2 \sin^2 kl + \cos^2 kl}$$

where $k = \frac{\omega}{a}$, and a is the velocity of sound.

From this equation and the values of $|Z|$ and ω from line 2 of Table I, $\frac{\alpha}{a\rho}$ was fixed at 1.5. This value was used for subsequent calculations, since the properties of the exit system were not changed. There is here the implicit assumption that α is not a function of the mean suction rate. Since α arises from losses in the exit pipe and venturi, it is clear that this is not exact, and this procedure amounts to a linearization.

With this value of α , one can compute Z^R and Z^I from the relations

$$\frac{Z^R}{a\rho} = \frac{\frac{\alpha}{a\rho}}{\left(\frac{\alpha}{a\rho}\right)^2 \sin^2 kl + \cos^2 kl} \quad \frac{Z^I}{a\rho} = \frac{\left[\left(\frac{\alpha}{a\rho}\right)^2 - 1\right] \cos kl \sin kl}{\left(\frac{\alpha}{a\rho}\right)^2 \sin^2 kl + \cos^2 kl}$$

and the phase angle θ , defined by $Z = |Z| e^{-i\theta}$ is given by

$$\tan \theta = \frac{-Z^I}{Z^R}$$

This calculation gives the value $\theta = 4.7^\circ$ for all suction rates with the large plenum configuration. Column 9 of Table I shows that this angle increases from 4 to 8° for low suction rate to something less than 30° for high suction rate. This change indicates that the assumption concerning constant α is not valid over a large range of suction rates. Indeed, if a larger value of α is used, the phase angle increases while $|Z|$ decreases, in keeping with columns 8 and 9 of Table I. For $\frac{\alpha}{a\rho} = 2.5$, we obtain $|Z| = .48$ and $\theta = 13^\circ$. This average value for α is probably better for the description of line 4, Table I. For the small suction plenum, using $f = 28.6$ from line 8 of Table I, and again using $\frac{\alpha}{a\rho} = 1.5$, the value of θ is calculated as 21.2° and $|Z| = 0.86$. The experimental value of θ is shown as less than 40° . The uncertainty here is associated with the irregularity of the oscillation for this nearly stable configuration, and the correct value could be anywhere from 20 to 40° . If one uses $\frac{\alpha}{a\rho} = 2.5$ in the calculation, θ is given as 45° and $|Z| = 0.76$. It was not possible to measure $|Z|$ with this irregular oscillation.

The next calculations concern the ratio $\frac{\xi_s}{\xi_e}$ as regards both magnitude and phase. The formula used was

$$\frac{\xi_s}{\xi_e} = \frac{\omega V}{aA_e} \left\{ \left[\frac{aA_e}{\omega V} + \frac{Z^I}{a\rho} \right] - i \frac{Z^R}{a\rho} \right\}$$

which can be obtained directly from Eqs. (28) and (30). This calculation is useful in determining a theoretical value for the frequency and in constructing a phase diagram of the flow. The values of $\left| \frac{\xi_s}{\xi_e} \right|$ for the large and small plenum are 4.23 and 2.16. The phase angle ϕ defined by $\frac{\xi_s}{\xi_e} = \left| \frac{\xi_s}{\xi_e} \right| e^{-i\phi}$ can thus be computed, and has a value of 81.6° for the large plenum and 85.5° for the small plenum. Again these calculations are based on $\frac{\alpha}{a\rho} = 1.5$.

With this information one can construct a diagram for the unstable flow, showing the magnitude and phase of the oscillation in the various parts of the system. The information in line 3 is used in the example below.

Consider a representation where the flow into the exit pipe is taken as the reference (with zero phase angle)

$$\xi_e = |\xi_e| e^{-i\omega t}$$

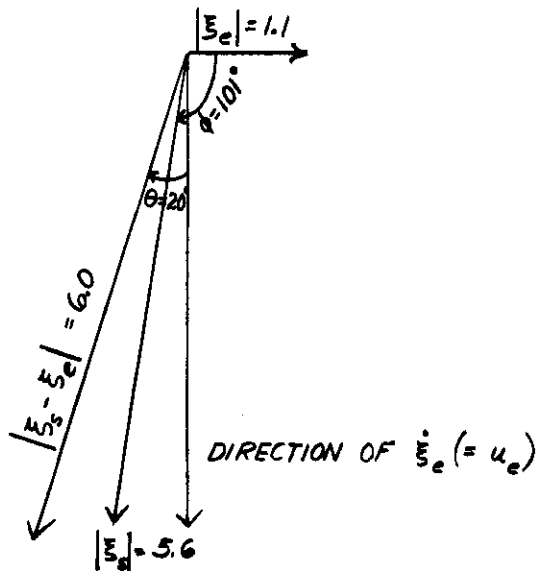
Because of the minus sign the diagram will rotate clockwise with increasing time. The exit flow rate, u_e , leads ξ_e by 90° , being given by

$$\dot{\xi}_e = -i\omega \xi_e = \omega \xi_e e^{-i\frac{\pi}{2}}$$

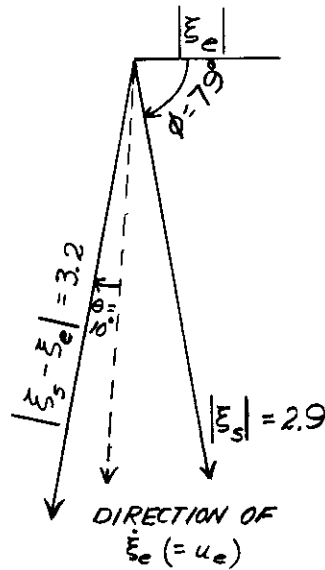
while ξ_s will lead ξ_e by the angle ϕ

$$\frac{\dot{\xi}_s}{\dot{\xi}_e} = \left| \frac{\dot{\xi}_s}{\dot{\xi}_e} \right| e^{-i\phi}$$

Taking the value of $\dot{\xi}_e$ from Table I and the information from the text above, we obtain the diagram



A similar diagram relating to the small plenum, line 8, appears as



SCALE: $|\xi_e| = 1$

The scale in the second diagram is arbitrarily taken as $|\xi_e| = 1$. In the experiments, ξ_e was too small to be measured accurately.

The frequency of oscillation can be calculated from formula (53), providing a check with the experimental value that was used in the calculation of α . The value for the large plenum oscillation (Refs. 2, 3, and 4) is 24.8 cycles/sec, in excellent agreement with the measured 24.6 cycles/sec. For the small plenum, however, the calculated frequency is 37 cycles/sec, considerably higher than the measured 28.6. This discrepancy has not been explained, and using a larger value of α does not appreciably change the calculated frequency. This is what would be expected from the constant measured values of the frequency in lines 2, 3, and 4.

In the text there is derived a criterion for the stability of the system, where the mass of the exit system is neglected. Although this condition is not exactly satisfied here, the criterion evolved describes the stability quite accurately. From Eq. (46) we have, for dynamic stability

$$1 - V \frac{\partial H_s}{\partial q_s} \frac{\partial p_e}{\partial q_e} \frac{A_s}{l_s \zeta_s} \frac{1}{(ap)^2} > 0 .$$

The value of this quantity is listed below, along with the observed stability, copied from Column 4 of Table I

Reference Number	Experimental Stability	Stability Measure	Reference Number	Experimental Stability	Stability Measure
1	No OSC.	-0.4	6	No OSC.	0.8
2	OSC.	-2.0	7	No OSC.	0
3	OSC.	-1.8	8	Some OSC.	-0.3
4	Some OSC.	-0.6	9	No OSC.	+0.1
5	No OSC.	0	10	No OSC.	-0.5

The stability measure should be positive in cases of no oscillation, and inspection of the table shows that this is the case in all but lines 1 and 10, where a small negative value is obtained. In experiment 1 the system could be put into oscillation by a small increase in suction rate. Line 10 (for the 1.0 inch slot) represents a case where there was no oscillation, but increasing the tunnel speed from 200 ft/sec to 250 ft/sec caused the oscillation to begin. The effect of tunnel speed on pressure recovery in the plenum is shown in Fig. 12. The curve for a tunnel speed of 80 ft/sec (for line 6 of Table I) is similar to that for 200 ft/sec tunnel speed, when pressures are plotted in units of $\frac{1}{2} \rho u_0^2$ and suction rate in units of boundary layer flow, but the actual value of $\partial H_s / \partial q_s$ in lb/ft²/ft³/sec is correspondingly lower for lower tunnel speeds. For this reason, increasing the tunnel speed to 250 ft/sec in line 10 can cause instability by virtue of the attendant increase in $\partial H / \partial q_s$. Line 9, with the 1.3 inch slot, shows a still lower value for plenum pressure recovery rate. In both this and the 1 inch slot, the static instability was very pronounced, including nonuniform flow distribution both spanwise and chordwise in the slot. It is concluded that these large flow asymmetries result in corresponding pressure losses, thus reducing the pressure recovered in the plenum.

The stability in line 7 results from a different cause, namely reducing the pressure available to the plenum chamber by changing the boundary-layer profile in the tunnel. When air is introduced through the tunnel wall ahead of the suction slot, the boundary layer in the tunnel takes on a laminar-like profile (see Fig. 8). The head available to the plenum is thereby reduced, as shown by the calculation of available head assuming no momentum loss. These graphs are shown in Fig. 13, and were calculated from the measured profiles. The experimental value of the head recovered in the plenum is graphed in Fig. 12. It is seen that the value of $\partial H_s / \partial q_s$ is only slightly greater than zero, resulting in dynamic stability. As discussed in the section on Static Stability, this change in boundary layer also resulted in more uniform velocity distribution across the slot.

Contrails

Finally, the energy balance for oscillatory systems can be checked by Eq. (52)

$$\left| \frac{\xi_s}{\xi_e} \right| = \sqrt{\frac{\partial p_c / \partial q_e}{\partial H_s / \partial q_s}}$$

In deriving this equation, it was assumed that $\frac{\partial p_c}{\partial q_e}$ and $\frac{\partial H_s}{\partial q_s}$ are constant over the cycle of oscillation. From the measured amplitude of oscillatory flow and the graphs of plenum pressure recovery, it is clear that this condition is not satisfied for $\frac{\partial H_s}{\partial q_s}$. If this is neglected and the comparison made using an average value for $\frac{\partial H_s}{\partial q_s}$ (averaged over the cycle as indicated in equations on page 13), one obtains

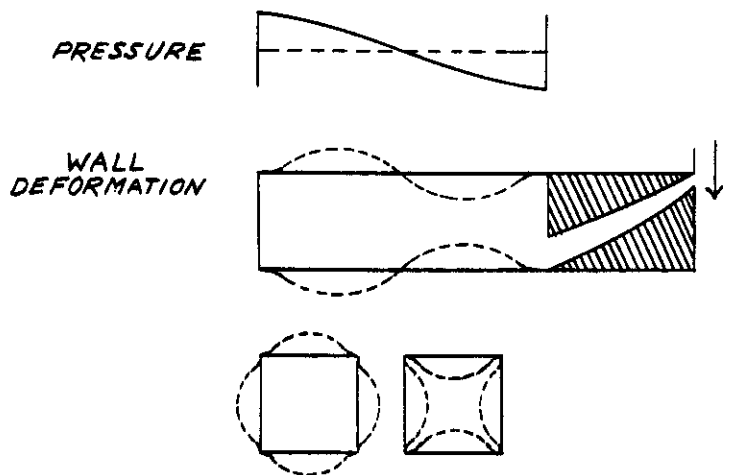
	Reference No.	$\left \frac{\xi_s}{\xi_e} \right $	$\sqrt{\frac{\partial p_c / \partial q_e}{\partial H_s / \partial q_s}}$
Large Plenum	2	4.2	5.4
	3	4.2	5.5
	4	4.2	7.4
Small Plenum	8	2.2	5.0

The value of $\left| \frac{\xi_s}{\xi_e} \right|$ comes from the calculation described on page 23 using the phase diagram. α / α_p is taken as $1.5(\alpha_p) / A_e$, and $\frac{\partial H_s}{\partial q_s}$ is given in column 11 of Table I. For the small plenum, we notice that $\left| \frac{\xi_s}{\xi_e} \right|$ must be smaller than for the large plenum, although the values of $\partial p_c / \partial q_e$ and $\partial H_s / \partial q_s$ should be the same for the two systems. This fact causes the small plenum to oscillate only at high values of $\partial H_s / \partial q_s$, and then with small amplitudes, giving a larger value for the average $\partial H_s / \partial q_s$. This decreases the ratio $\sqrt{\frac{\partial p_c / \partial q_e}{\partial H_s / \partial q_s}}$. It appears that for this small oscillation, our relatively coarse measurement of $\partial H_s / \partial q_s$ rather underestimates the proper value. However, it is this energy condition that determines the amplitude of the oscillation, all other conditions being concerned only with ratios of the oscillation in various components of the system. In order to appreciate this, it must be realized that $\partial H_s / \partial q_s$ is actually a function of q_s , so that as q_s becomes larger the "effective" value of $\partial H_s / \partial q_s$ becomes smaller and will eventually change sign.

During the early measurements of dynamic instability, a strong, high frequency oscillation occurred, completely masking the normal oscillations described in this section. The frequency of this oscillation was measured at 175 cycles/sec and it caused a violent vibration of the plenum walls. It was found that if the plenum walls were held firmly this oscillation disappeared, and the normal oscillation returned. It was concluded that this difficulty was associated with the natural frequency of the plenum walls, and calculations (described briefly below)

bear this out. Accordingly, the sides of the plenum were braced with 3/4 inch angle iron, and the high frequency oscillation did not recur.

In the calculation of the natural frequency of the walls of the plenum, it was known that the internal length of the plenum (from the end to the diffuser blocks) was 3.0 feet, or very close to 1/2 wavelength for standing waves of the high frequency inside the plenum. Further, it was known that bracing the side walls of the plenum stopped the oscillation. Thus the suspected mode of oscillation was one where the side walls of the plenum vibrate with the first mode in the short dimension and the second mode in the long dimension. In this case the vibration of the walls is similar to the pressure vibration, allowing a coupling between the two. The boundary conditions are those of a clamped plate, since a twisting mode of vibration (corresponding to simply supported edges) does not allow for a volume change in the plenum. This volume change is similarly required for energy to be transferred between the air and the walls. The mode is illustrated in the sketch below:



To calculate the natural frequency, the walls were first considered as simply supported plates. The frequency contribution from each dimension was then corrected as one would correct for the corresponding uniform beam. The resultant calculated frequency is 193 cycles/sec, compared to the measured value of 175 cycles/sec.

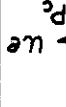
The following conclusions have been arrived at as a result of the present investigation. These supplement those of Reference 1.

- (1) The dynamic instability encountered in the tests described in this report (regular oscillations of the flow in air induction systems ingesting boundary layer air) could be eliminated by reducing system volume. The criterion for maximum system volume allowable for dynamic stability could be predicted with fair accuracy theoretically, using inlet characteristics measured under static conditions.
- (2) For the systems tested in this investigation, reduction of the slope of the curve of total head vs. volume flow produced by change of the boundary-layer velocity profile from turbulent to laminar-like was sufficient to produce dynamic stability and eliminate system oscillation. The critical value of this slope could be predicted theoretically.
- (3) The slope reduction referred to in (2) was also sufficient in the present systems to practically eliminate static instability (unequal flow rates in identical parallel branches of the system).
- (4) With a turbulent velocity profile, none of several simple schemes of interconnecting twin ducts described herein was capable of eliminating static instability.
- (5) Measurements of inlet characteristics made under nonoscillatory conditions proved adequate for calculation of dynamic characteristics as evidenced by agreement between several calculated and measured results for oscillatory conditions.
- (6) Structural deformation of the duct system may be coupled to the air in the duct system to produce violent oscillations of the duct walls at a frequency near the structural frequency under certain conditions. This matter was not investigated in detail; the oscillation was eliminated by stiffening the duct wall.
- (7) When regular oscillation of the duct system occurred, it was at a frequency generally in good agreement with acoustic theory. The simple Helmholtz resonator theory is adequate when all ducts are short compared to $1/4$ the wavelength of the sound waves involved in the oscillation. For longer ducts, such as that used as an exit pipe in the present tests, the more complete theory of wave propagation in tubes must be applied.

Contrails
BIBLIOGRAPHY

1. Flax, A. H., Treanor, C. E., and Curtis, J. T. Stability of Flow in Air-Induction Systems for Boundary-Layer Suction. WADC TR 53-189.
2. Wieghardt, K. Versuchseinrichtung zur Erzeugung dicker Laminarschichten. ZWB, Untersuchungen und Mitteilungen No. 6610, July 19, 1944. Translated by NACA, File No. 51 N-25342, April 1953.
3. Pfenninger, W. Experiments on a Laminar Suction Airfoil of 17 Per Cent Thickness. Journal of the Aeronautical Sciences. Volume 16, Number 4. April 1949. pp. 227-236.
4. Dickinson, H. B. Flight and Tunnel Test Research on Boundary-Layer Control. Journal of the Aeronautical Sciences, Volume 16, Number 4. April 1949. pp. 243-251.
5. Smith, A. M. O. and Roberts, Howard E. The Jet Airplane Utilizing Boundary-Layer Air for Propulsion. Journal of the Aeronautical Sciences. Volume 14, Number 2. February 1947. pp. 97-109.
6. von Doenhoff, A. E. and Loftin, L. K. Jr. Present Status of Research on Boundary-Layer Control. Journal of the Aeronautical Sciences. Volume 16, Number 12. December 1949. pp. 729-740.
7. Den Hartog, J. P. Mechanical Vibrations. Second Edition. McGraw-Hill Book Company, Inc. 1940.
8. Letter from A. M. O. Smith, Douglas Aircraft Company, Inc. to J. M. Gwinn, Cornell Aeronautical Laboratory, Inc. dated December 1949.
9. Martin, Norman J. and Holzhauser, Curt A. Analysis of Factors Influencing the Stability Characteristics of Symmetrical Twin-Intake Air-Induction Systems. NACA TN 2049. March 1950.
10. Rayleigh, John William Strutt, Baron The Theory of Sound. Second Edition. Revised and Enlarged. Dover Publications. 1945.
11. Morse, P. M. Vibration and Sound. Second Edition. McGraw-Hill Book Company, Inc. 1948.
12. Kamrass, M. Calibration of the C.A.L. High-Speed Wind Tunnel. Cornell Aeronautical Laboratory Report CAL/CF-771. January 1948.

TABLE 1
MEASUREMENTS CONCERNING DYNAMIC STABILITY

1	2A	2B	2C		2D	3	4	5	6	7	8	9	10	11
			BOUNDARY LAYER	PLENUM VOLUME (FT ³)										
REFERENCE NUMBER	SLOT WIDTH (INCHES)	PLENUM VOLUME (FT ³)	BOUNDARY LAYER	TUNNEL SPEED (FT/SEC)	SUCTION RATE	EXPERIMENTAL STABILITY	PLENUM MEASUREMENT OF $\frac{L_e}{L_c}$ ((FT ³))	EXIT PIPE MEASUREMENT OF $\frac{L_e}{L_c}$ ((FT ³ /SEC))	$\frac{ E_s - E_c }{L_e}$	EXIT PIPE IMPEDANCE $\frac{p_a Z}{\rho a^2}$	IMPEDANCE PHASE θ 	FREQUENCY OF OSCILLATION f (CYCLES/SEC)	INLET PRESSURE RECOVERY $\frac{\Delta H}{\rho H} \left(\frac{LB/FT^2}{FT^3/SEC} \right)$	
1	0.5	3.54	TURBULENT	200	0.8	NO OSC								0.7
2	0.5	3.54	TURBULENT	200	1.9	OSC.	.015	0.6 ± .1	3.85	.72	4 → 8°	24.6	1.5	
3	0.5	3.54	TURBULENT	200	3.4	osc	.025	1.0 ± .1	3.85	.68	< 15°	24.6	1.4	
4	0.5	3.54	TURBULENT	200	5.4	SOME OSC.	.012	0.8 ± .3	2.3	.47	< 30°	24.6	0.8	
5	0.5	3.54	TURBULENT	200	5.8	NO OSC.							0	
6	0.5	3.54	TURBULENT	80	3.0	NO OSC.							.09	
7	0.5	3.54	LAMINAR-LIKE	200		NO OSC.							.50	
8	0.5	1.4	TURBULENT	200		SOME OSC.					< 40°	28.6	1.6	
9	1.3	3.54	TURBULENT	200		NO OSC.								
10	1.0	3.54	TURBULENT	200		NO OSC.								

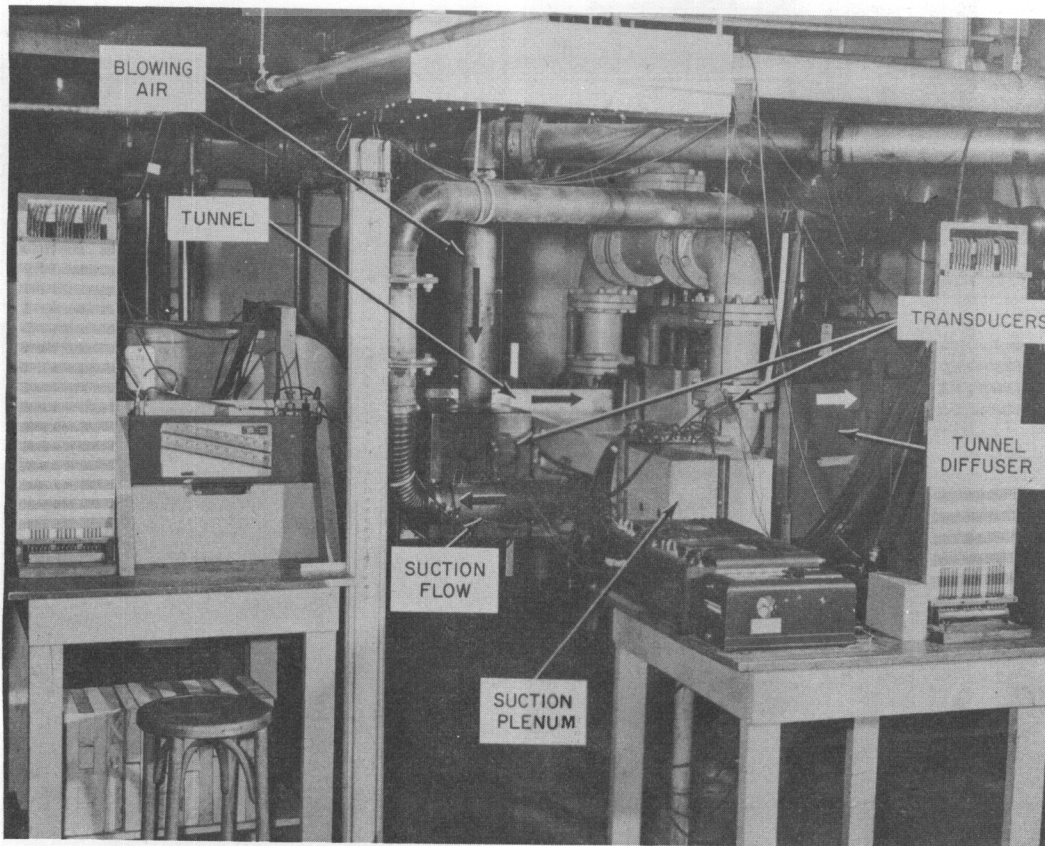


Figure 1 - GENERAL VIEW OF TEST EQUIPMENT

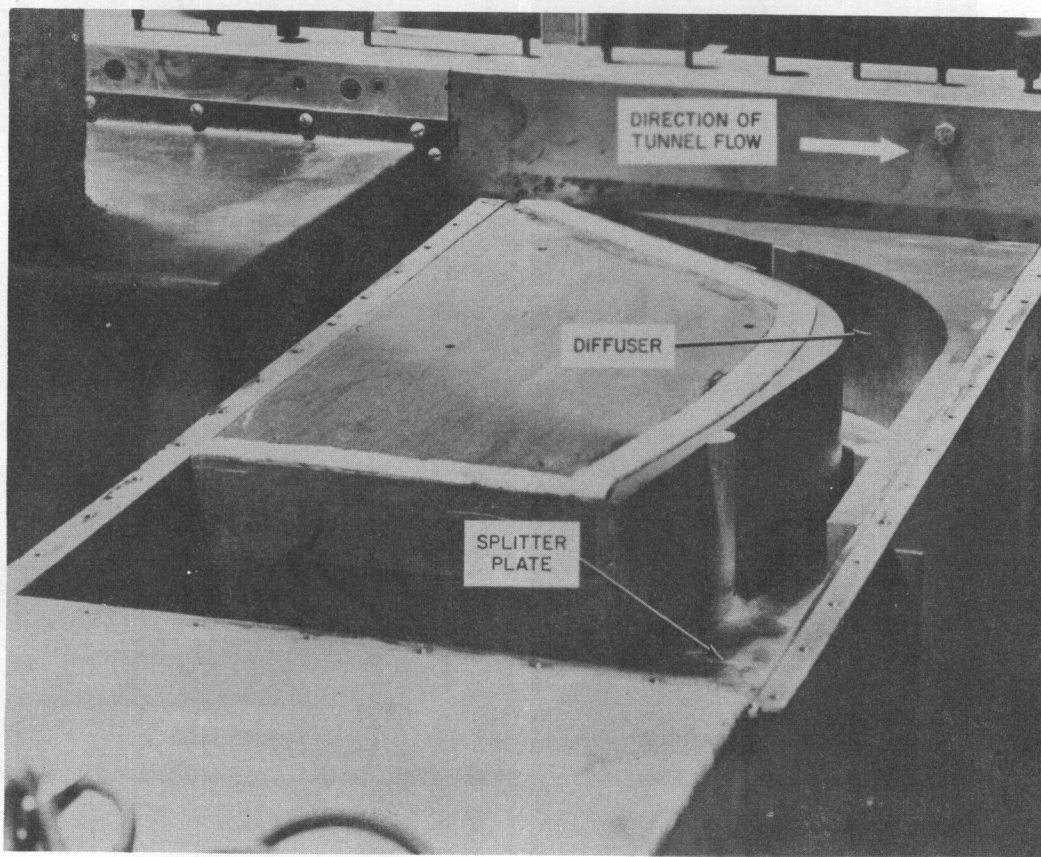


Figure 2 - SUCTION PLENUM WITH COVER REMOVED

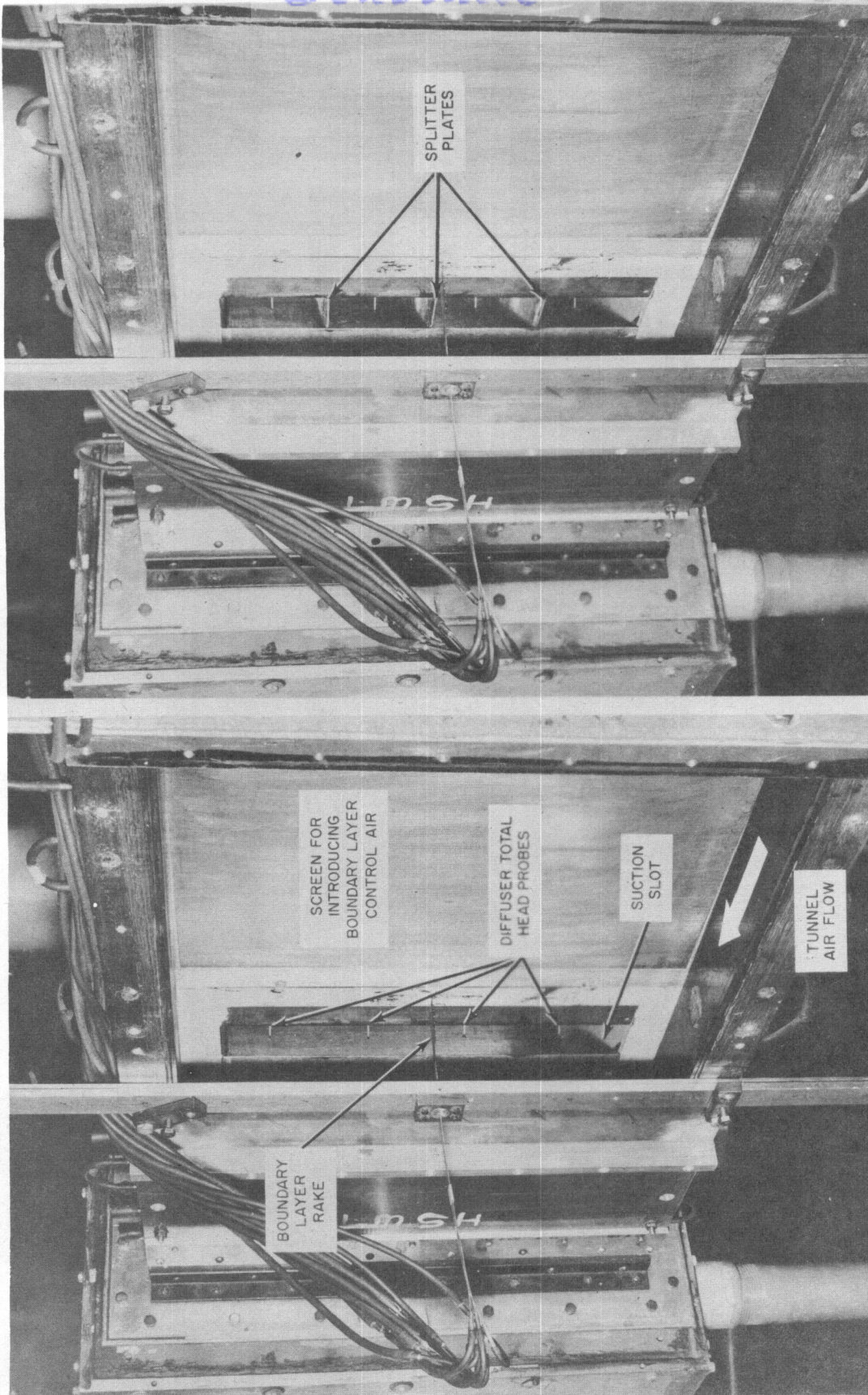


Figure 3 - TUNNEL WALL REMOVED (INSIDE WALL VIEW, SHOWING SUCTION SLOT WITHOUT SPLITTERS)

Figure 4 - TUNNEL WALL REMOVED (INSIDE WALL VIEW, SHOWING SUCTION SLOT WITH SPLITTERS)

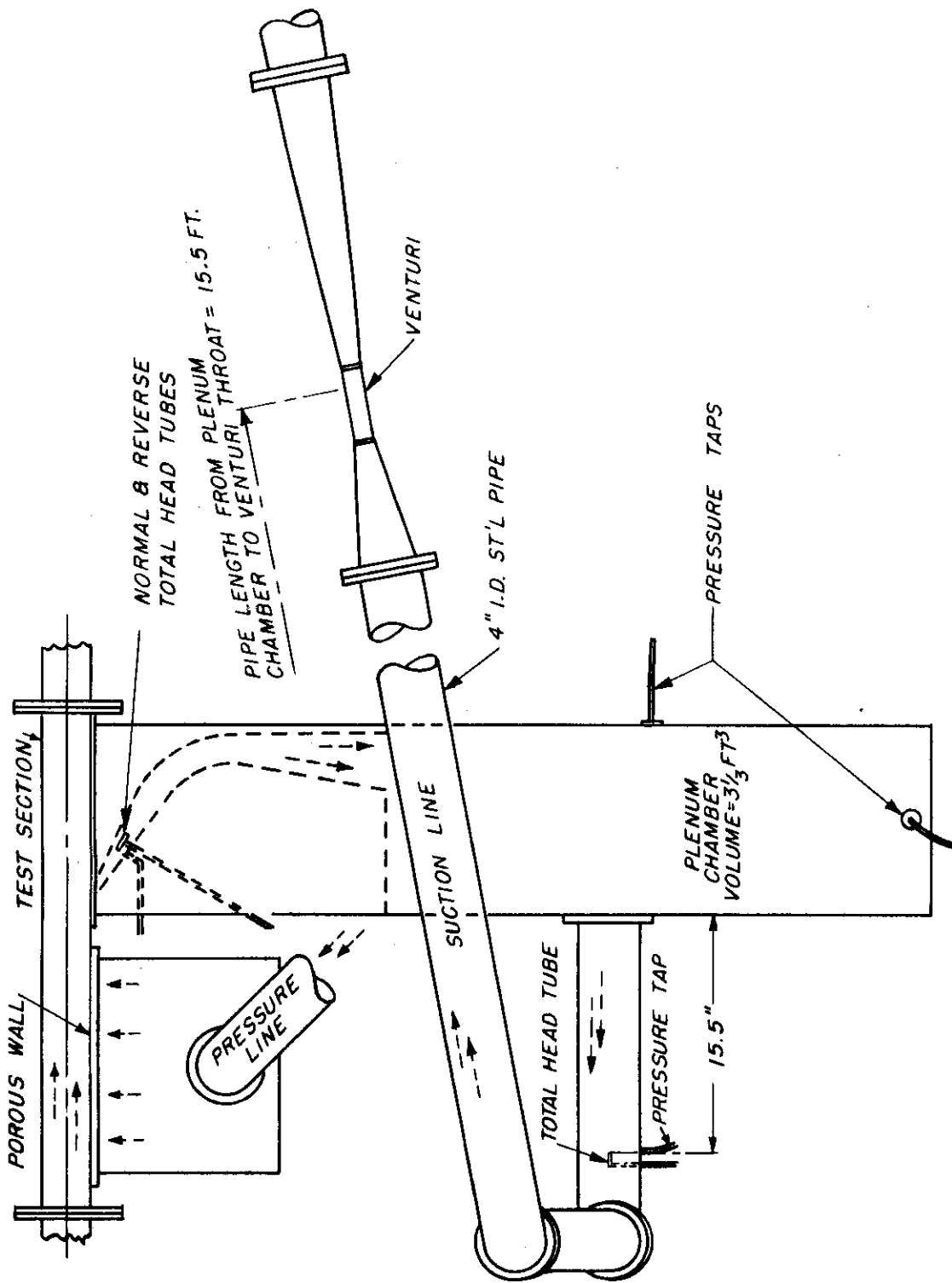


FIGURE 5a DIAGRAM OF SUCTION SYSTEM

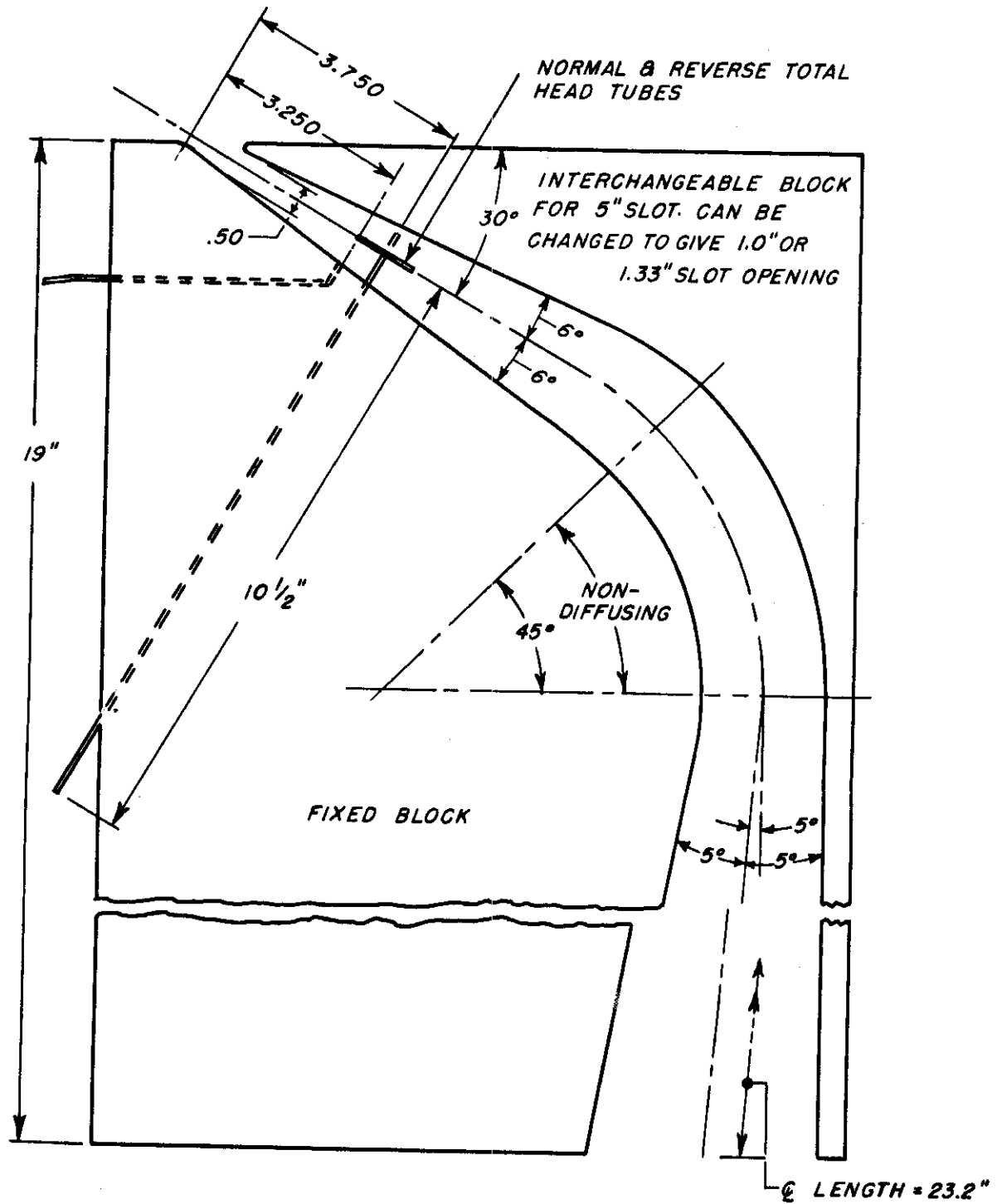


FIGURE 5b DETAIL OF SLOT AND DIFFUSER GEOMETRY

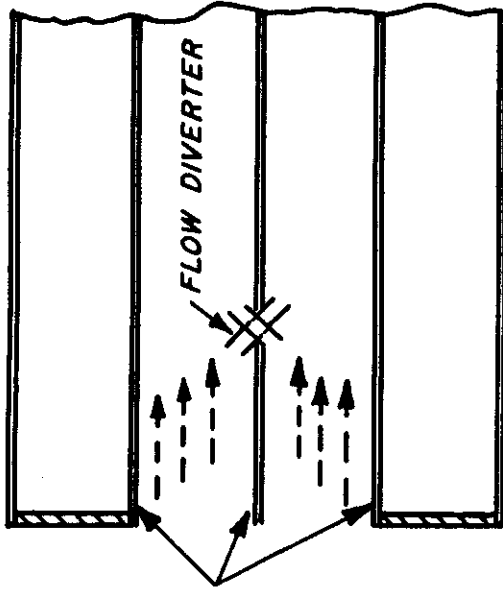


FIGURE 5e - DOUBLE DIVERTER

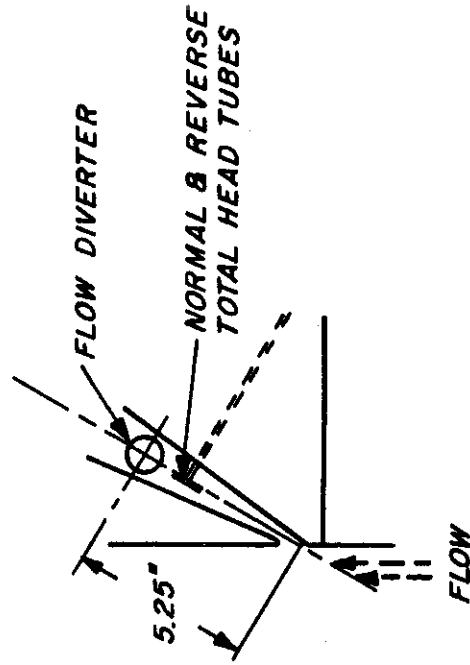


FIGURE 5f - LOCATION OF FLOW DIVERTER IN SLOT

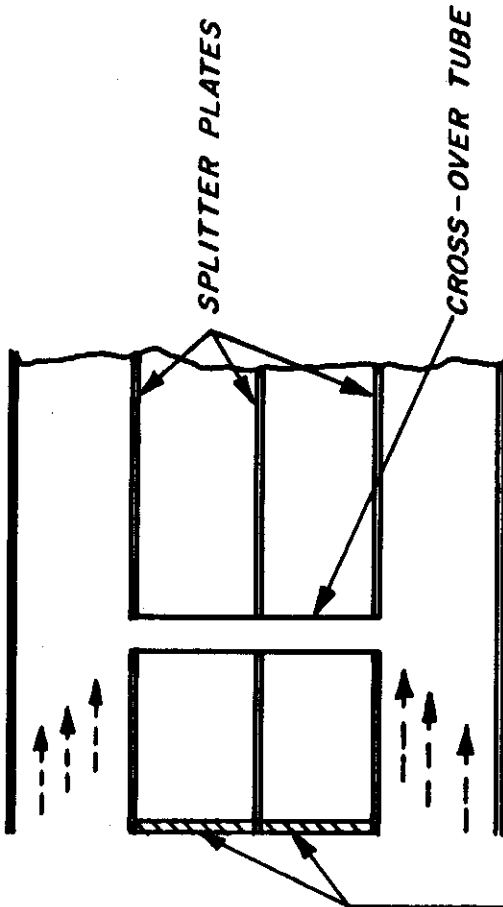


FIGURE 5c - INTERCONNECTING TUBE

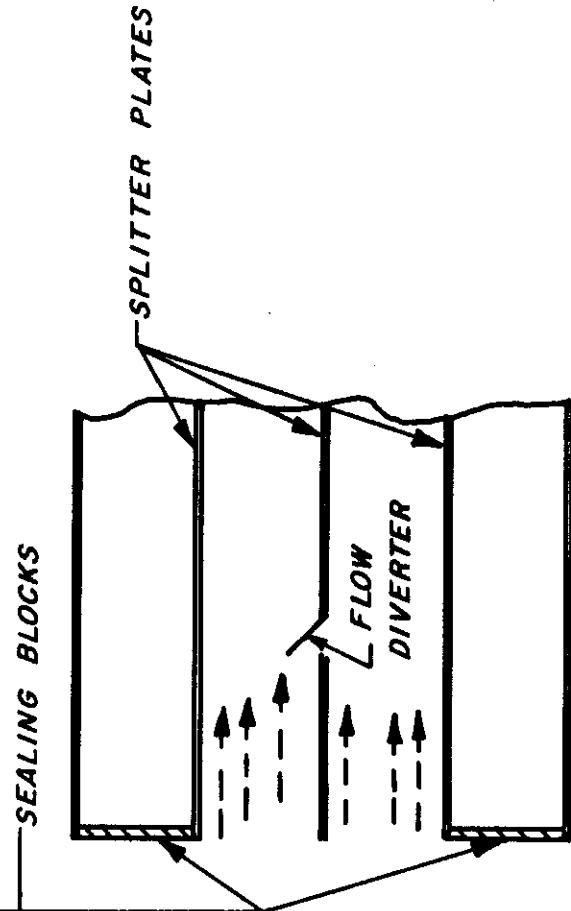
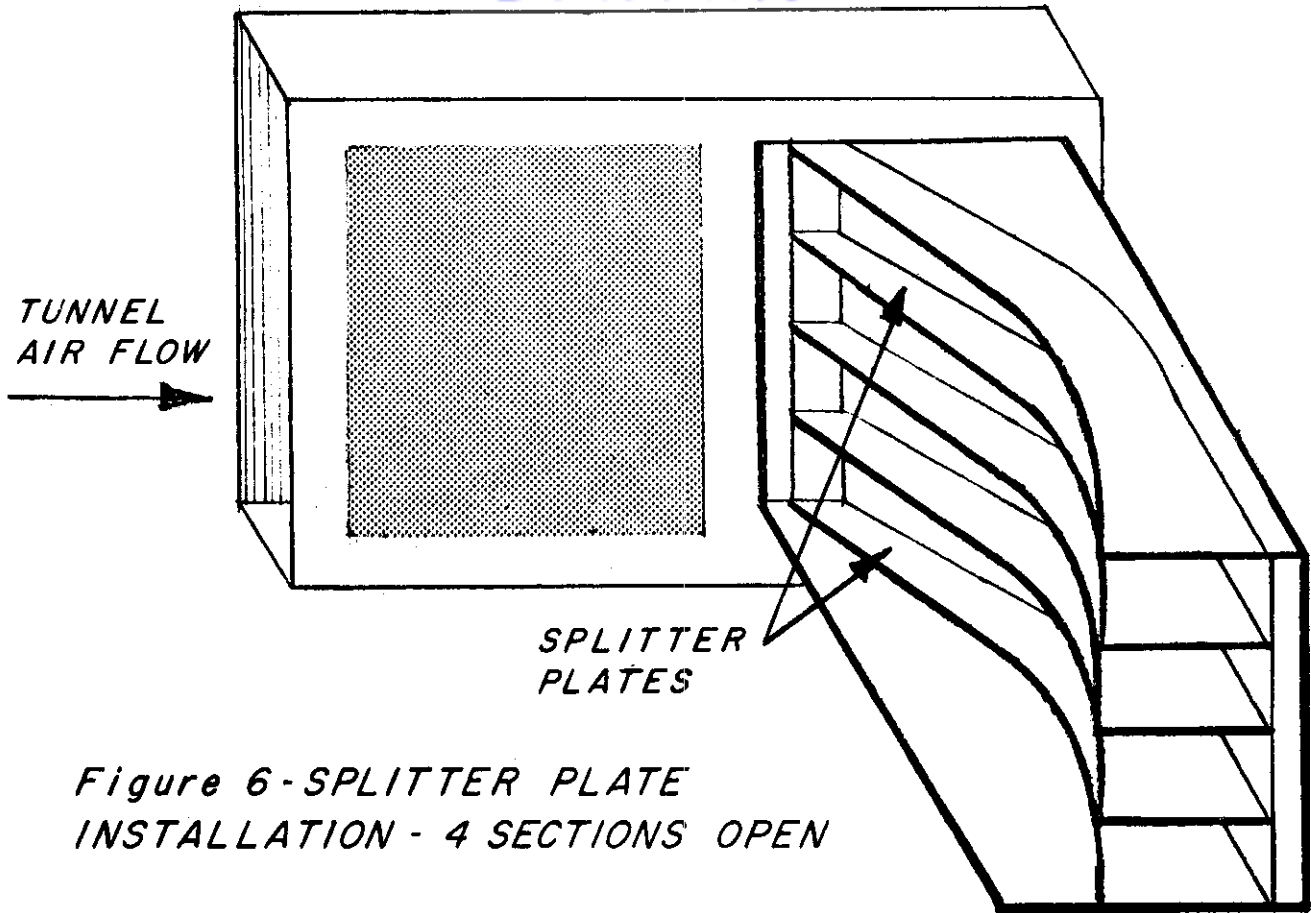
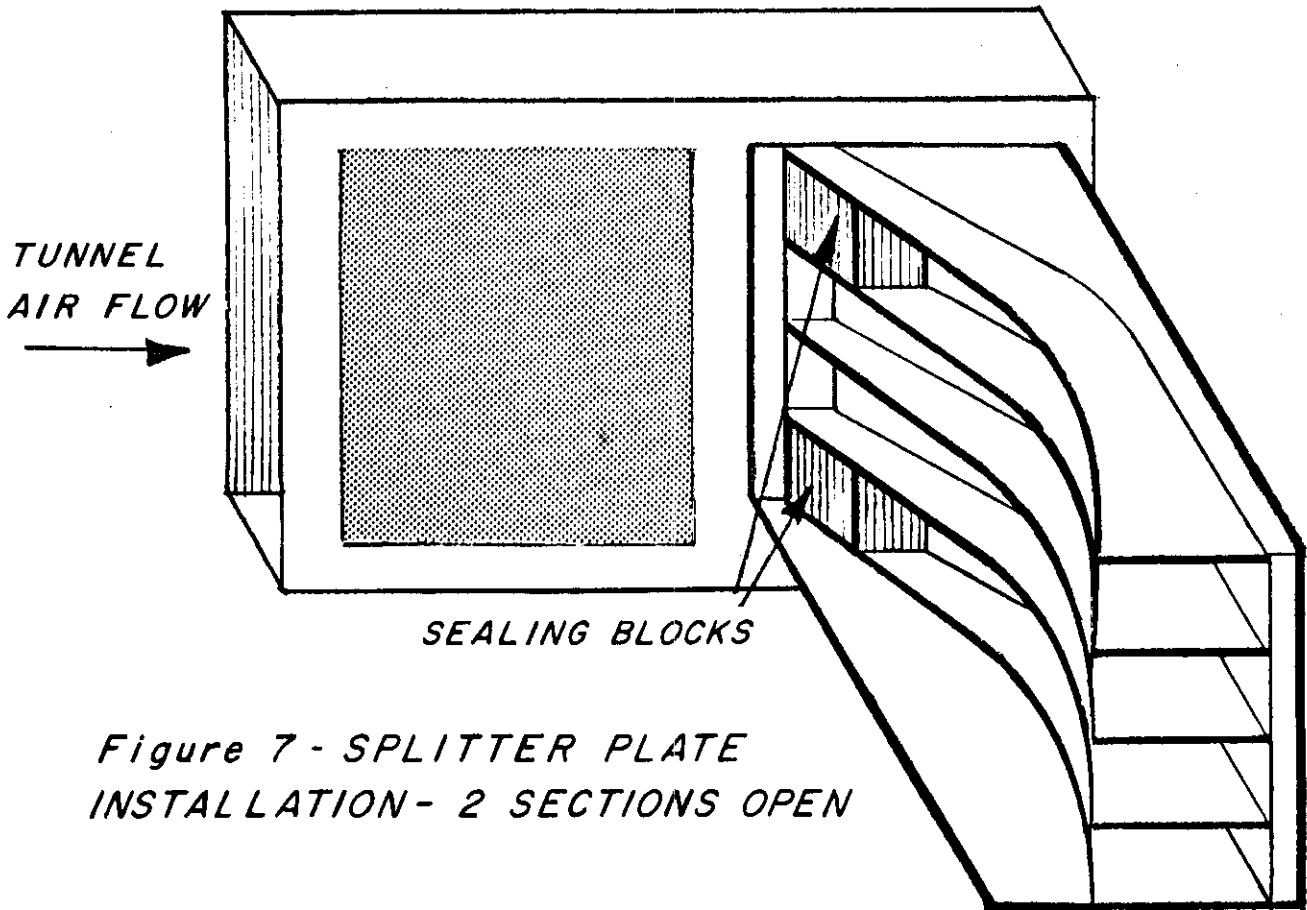


FIGURE 5d - 1" 45° DIVERTER



*Figure 6 - SPLITTER PLATE
INSTALLATION - 4 SECTIONS OPEN*



*Figure 7 - SPLITTER PLATE
INSTALLATION - 2 SECTIONS OPEN*

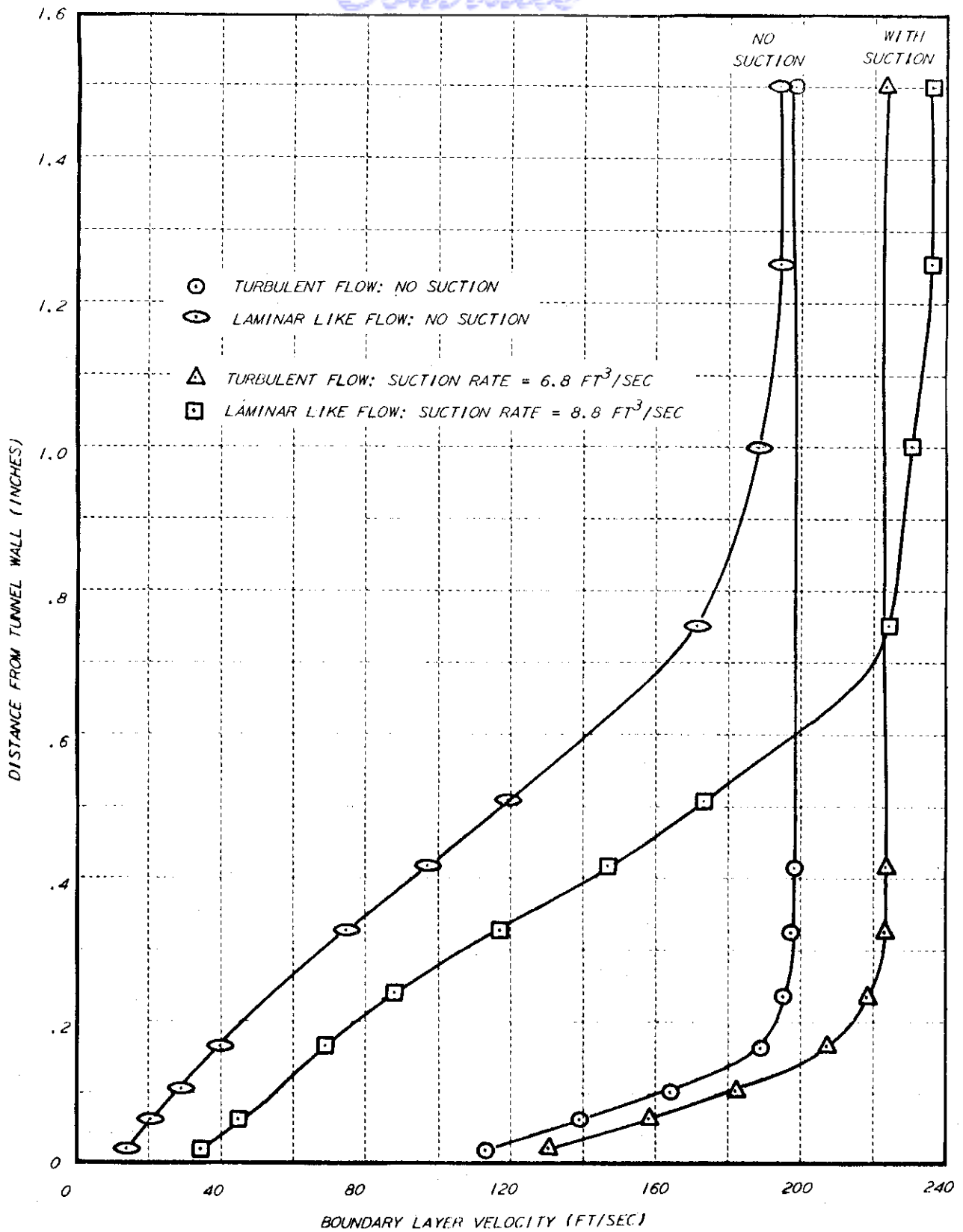


FIGURE 8 EFFECT OF BOUNDARY LAYER SUCTION ON FREE STREAM VELOCITY AND BOUNDARY LAYER PROFILE

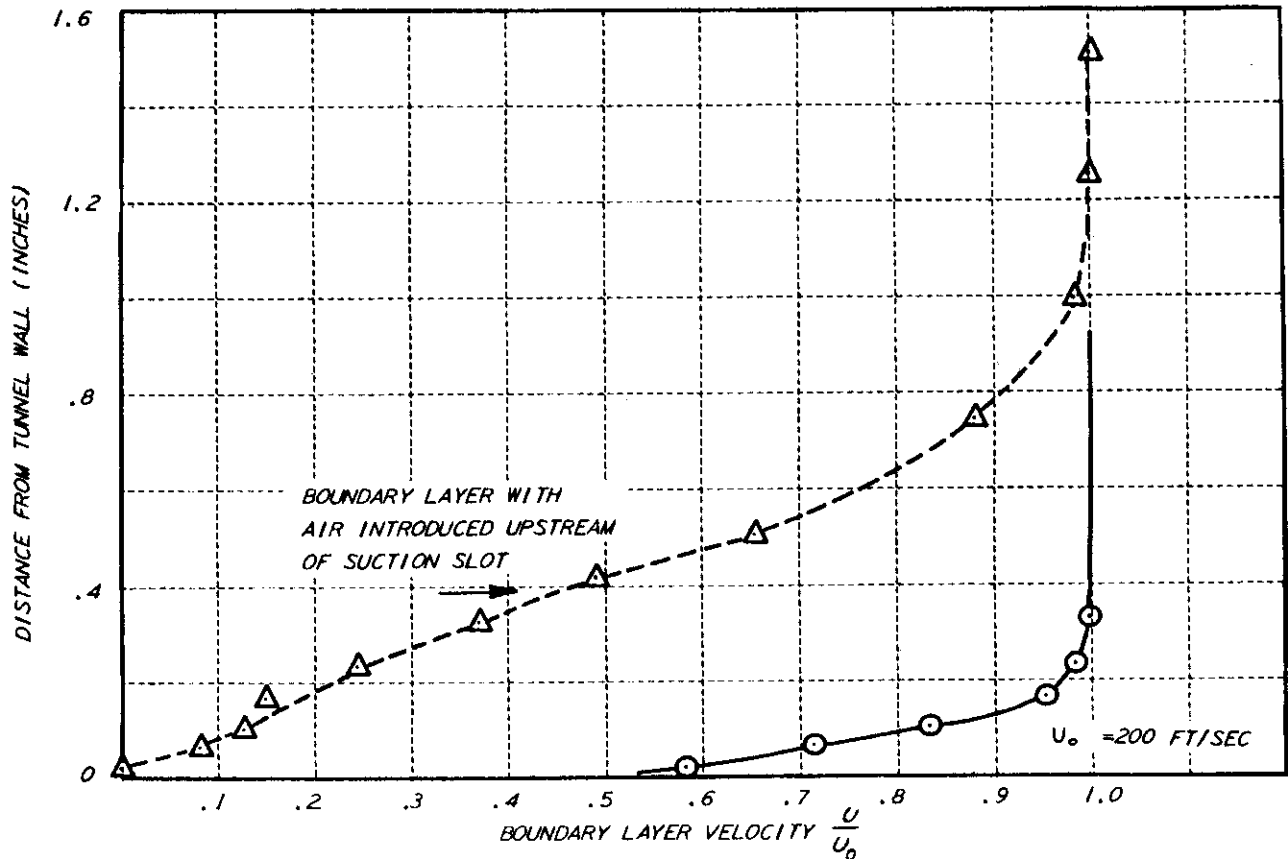
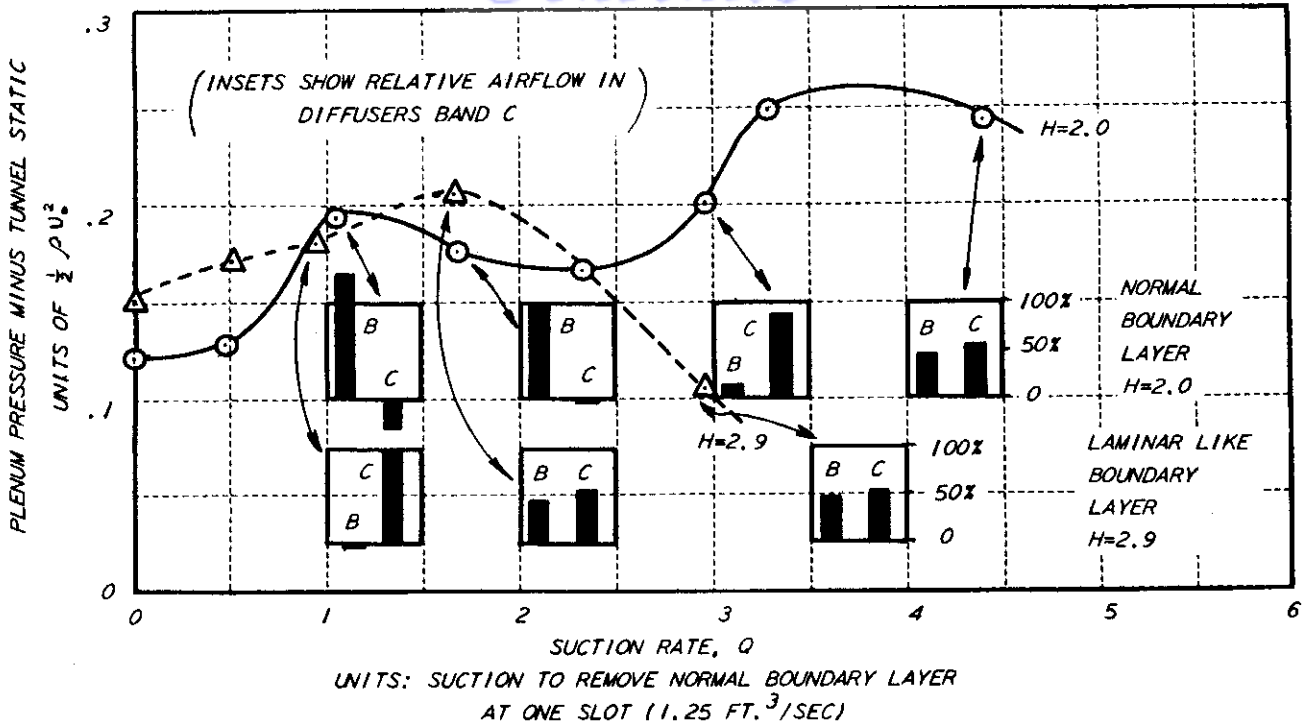


FIGURE 9 EFFECT OF BOUNDARY LAYER PROFILE ON STATIC STABILITY (TWO-SLOT SYSTEM)

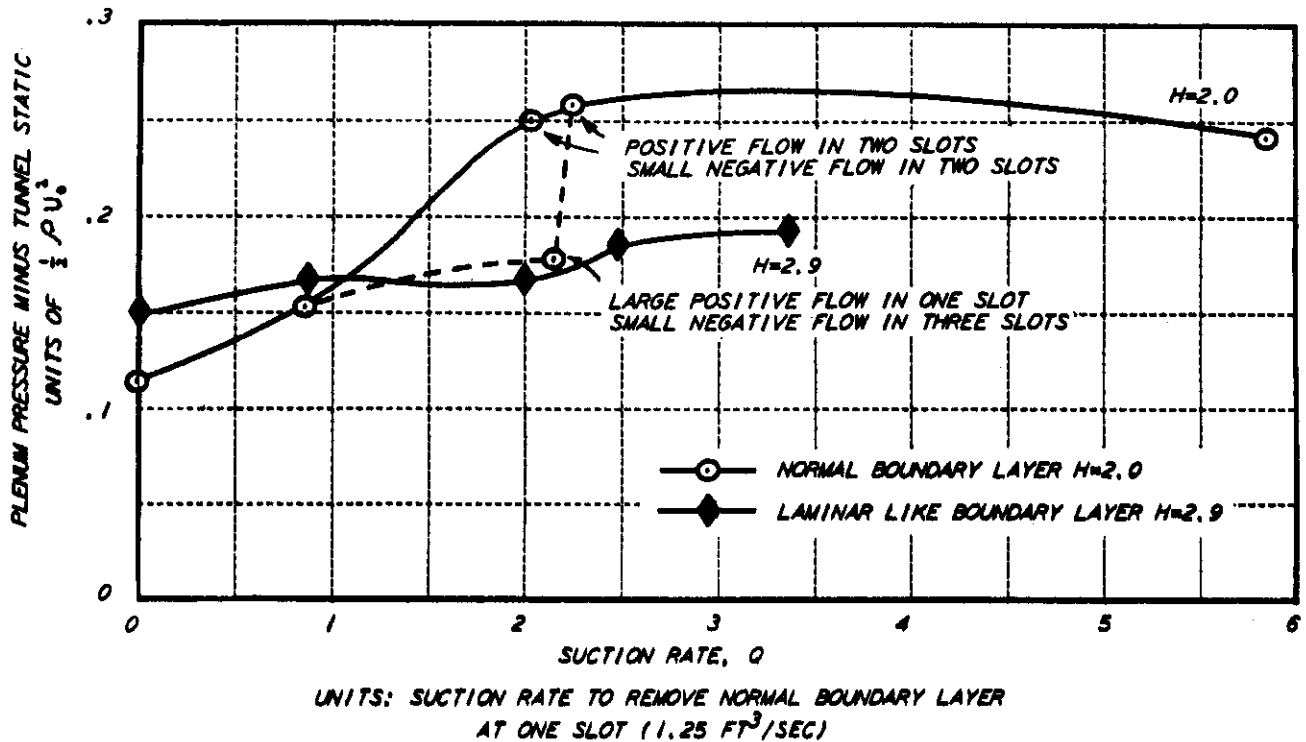
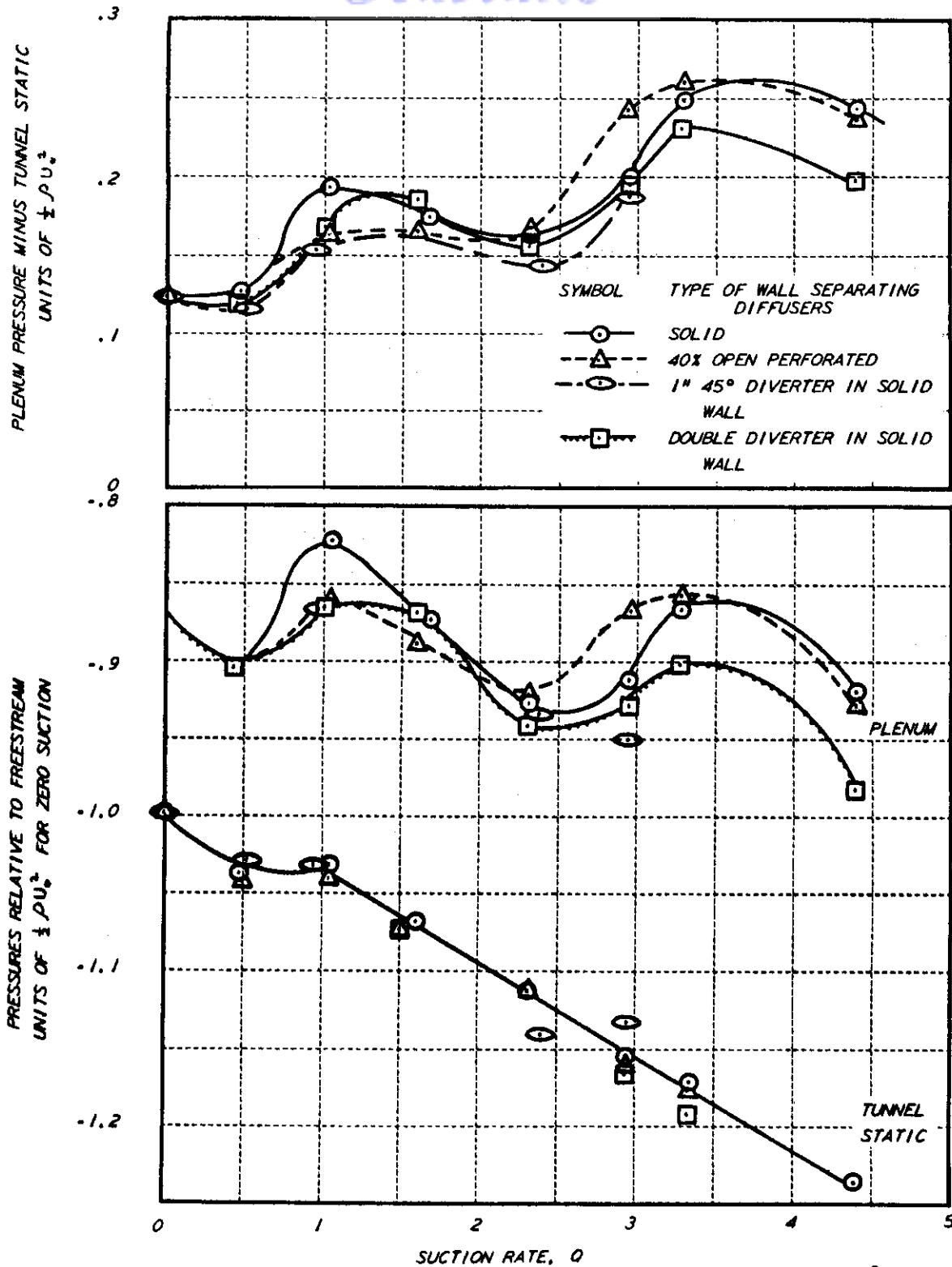


FIGURE 10 EFFECT OF BOUNDARY LAYER PROFILE ON PRESSURE RECOVERED IN PLENUM (FOUR-SLOT SYSTEM)

Contrails



UNITS: SUCTION RATE TO REMOVE NORMAL BOUNDARY LAYER AT ONE SLOT ($1.25 \text{ FT}^3/\text{SEC}$)
 FIGURE 11 PRESSURE VARIATIONS WITH TWO-SLOT SYSTEM WITH VARIOUS SCHEMES TO ALLEVIATE STATIC INSTABILITY

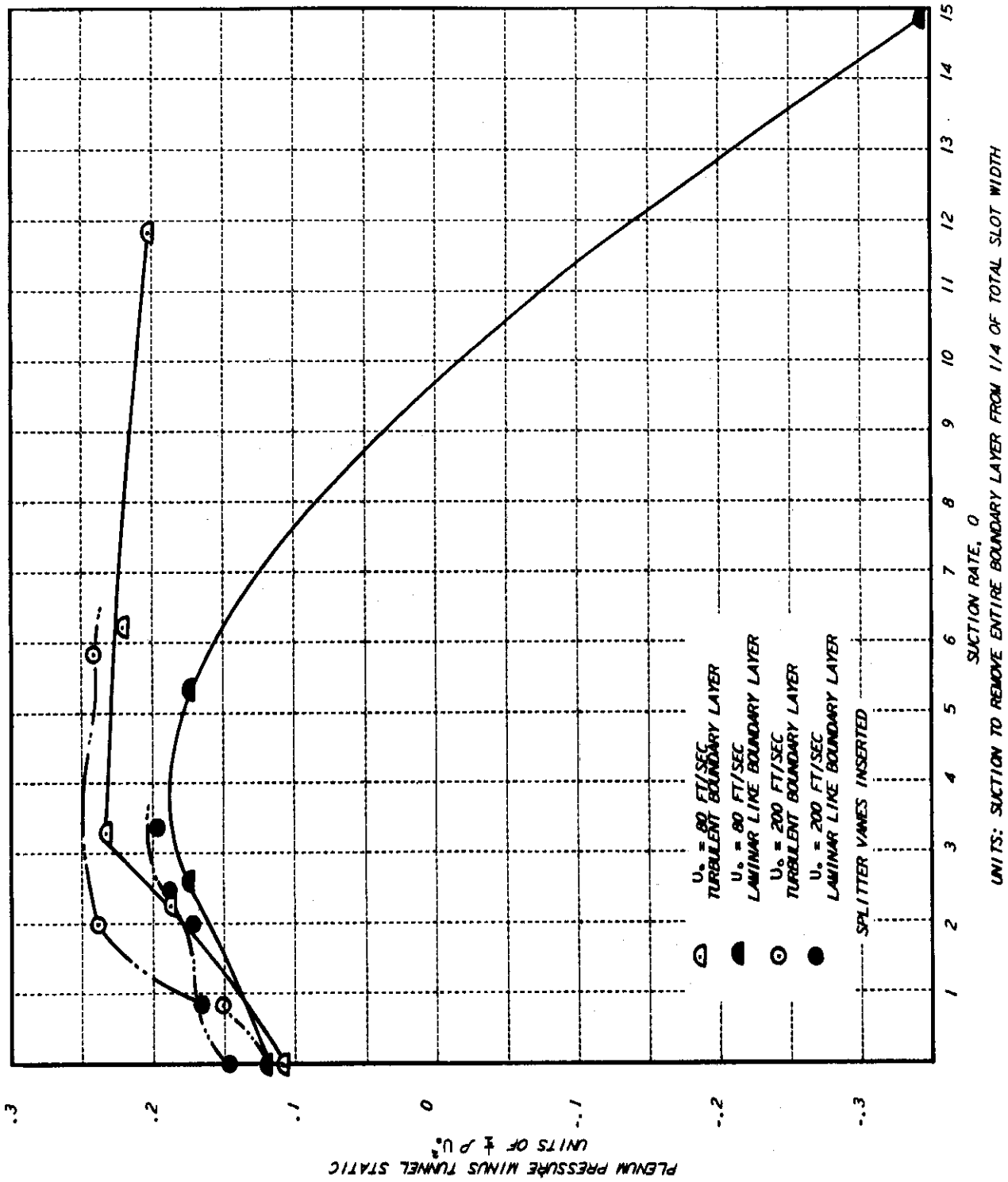
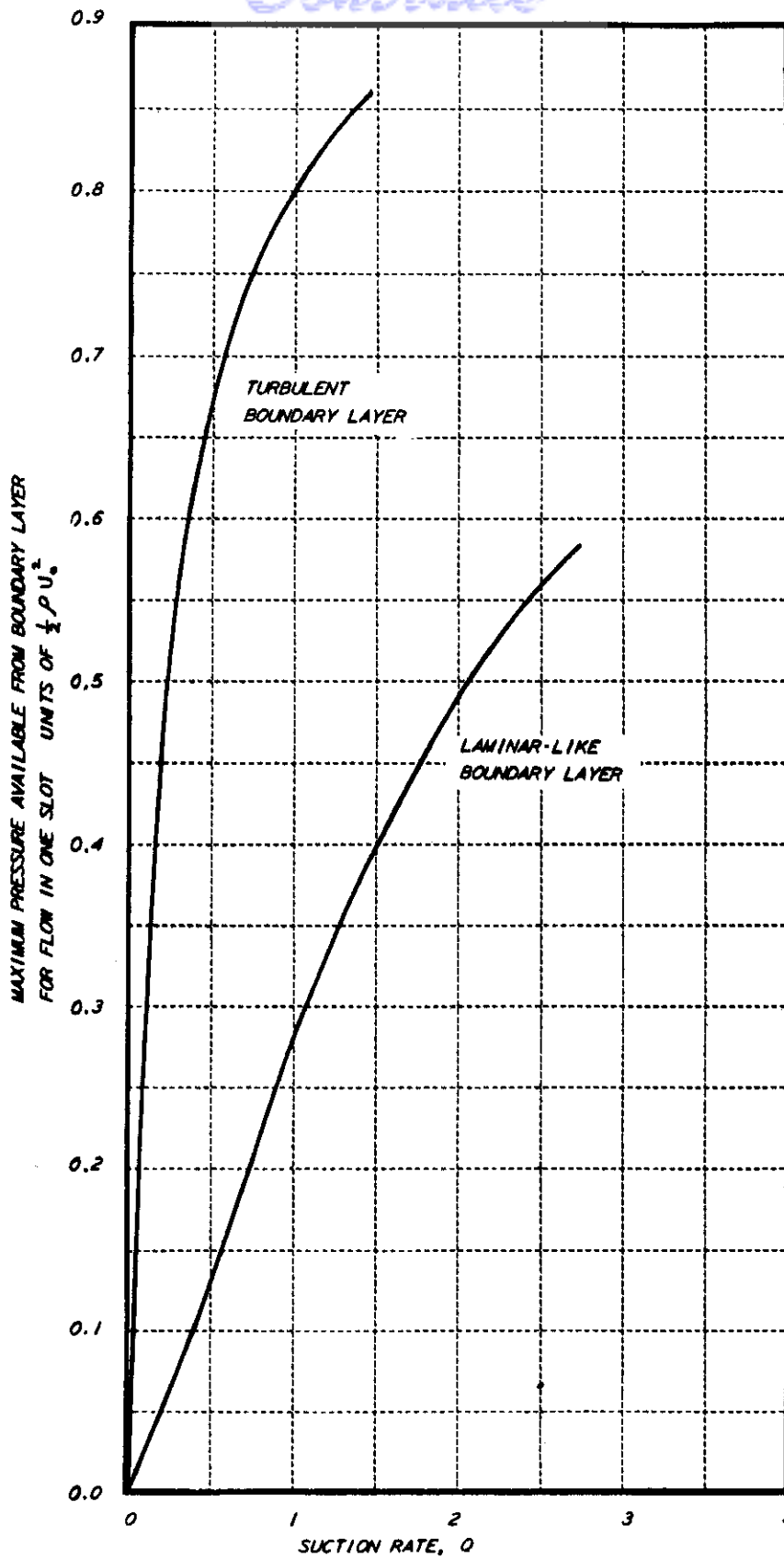


FIGURE 12 EFFECT OF TUNNEL VELOCITY AND BOUNDARY LAYER SHAPE ON PRESSURE RECOVERED IN PLENUM

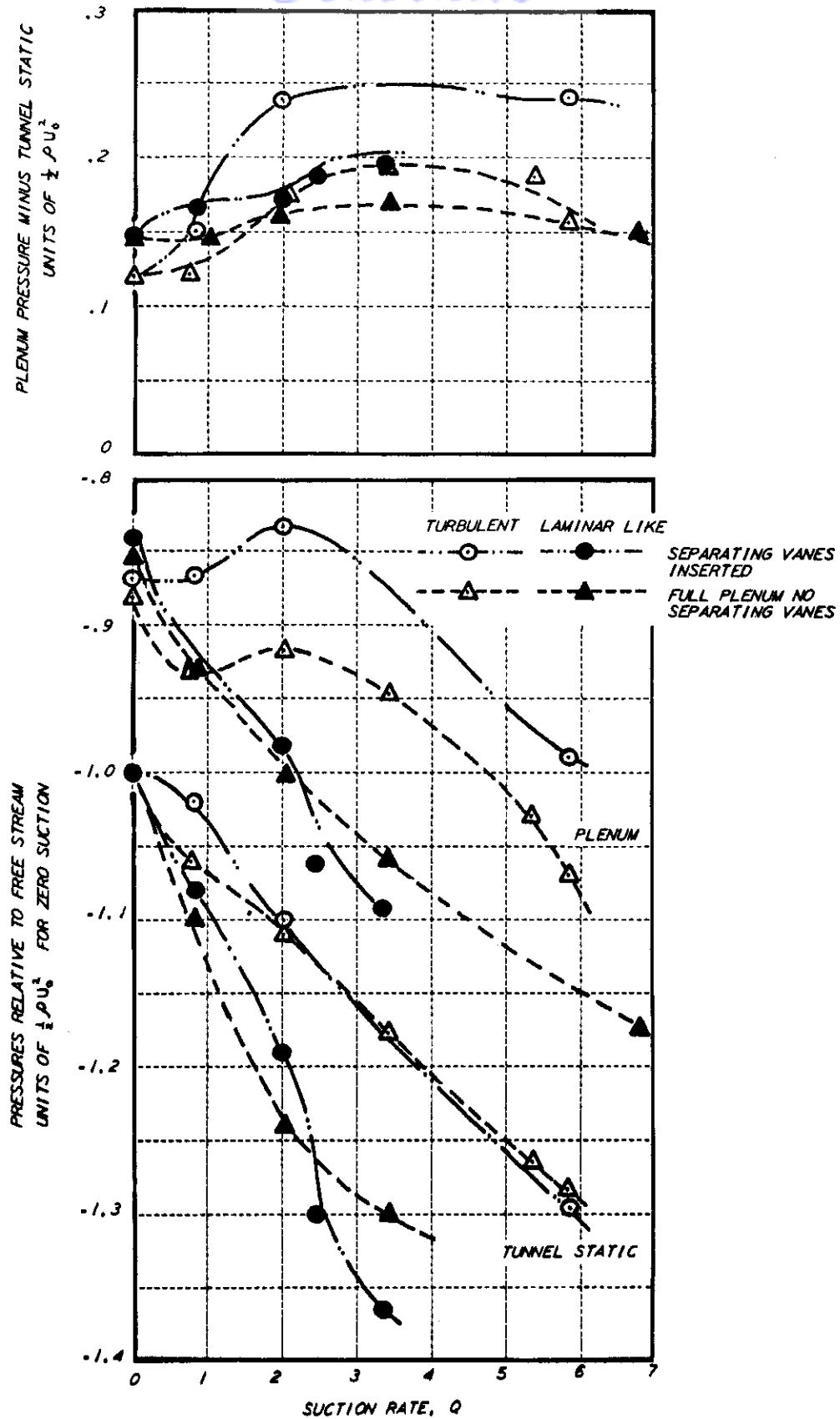
Contrails



UNITS: SUCTION RATE TO REMOVE NORMAL BOUNDARY LAYER AT ONE SLOT (1.25 FT³/SEC)

FIGURE 13 MAXIMUM AVAILABLE PRESSURE CALCULATED FROM MOMENTUM OF BOUNDARY LAYER

Contrails

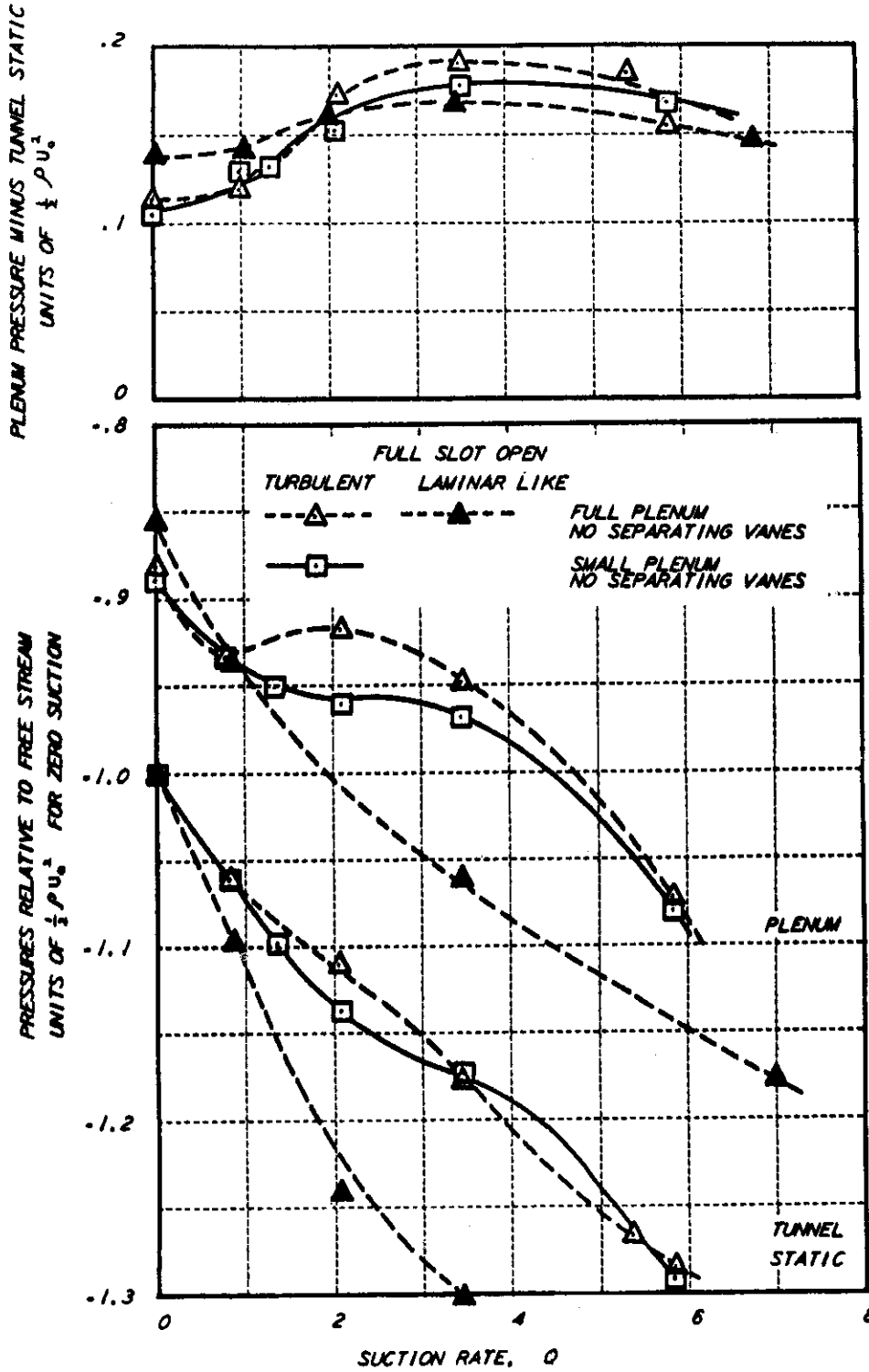


UNITS: SUCTION TO REMOVE TURBULENT BOUNDARY LAYER FROM 1/4 OF TOTAL SLOT WIDTH (11.25 FT³/SEC)

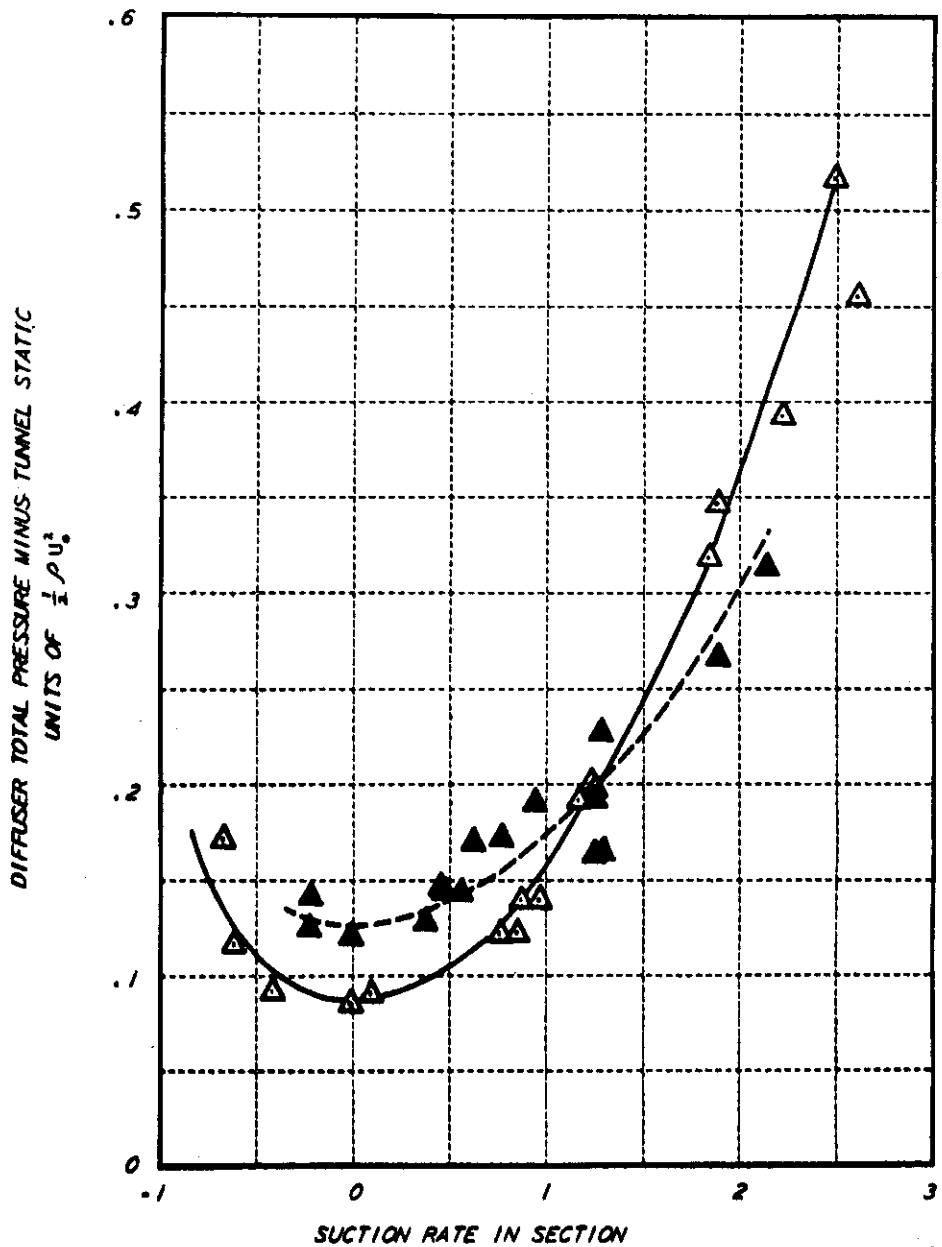
FIGURE 14 EFFECT OF SPLITTER PLATES ON PRESSURE

RECOVERED IN PLENUM

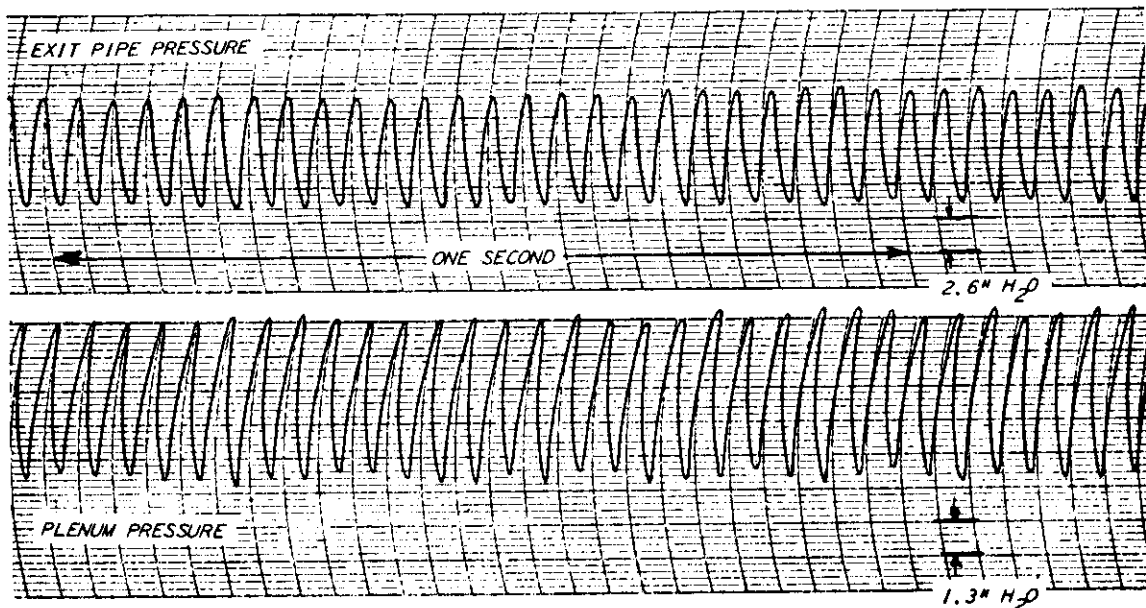
Contrails



UNITS: SUCTION TO REMOVE TURBULENT BOUNDARY LAYER FROM 1/4 OF TOTAL SLOT WIDTH (1.25 FT³/SEC)
 FIGURE 15 EFFECT OF PLENUM VOLUME ON PRESSURE RECOVERED IN PLENUM

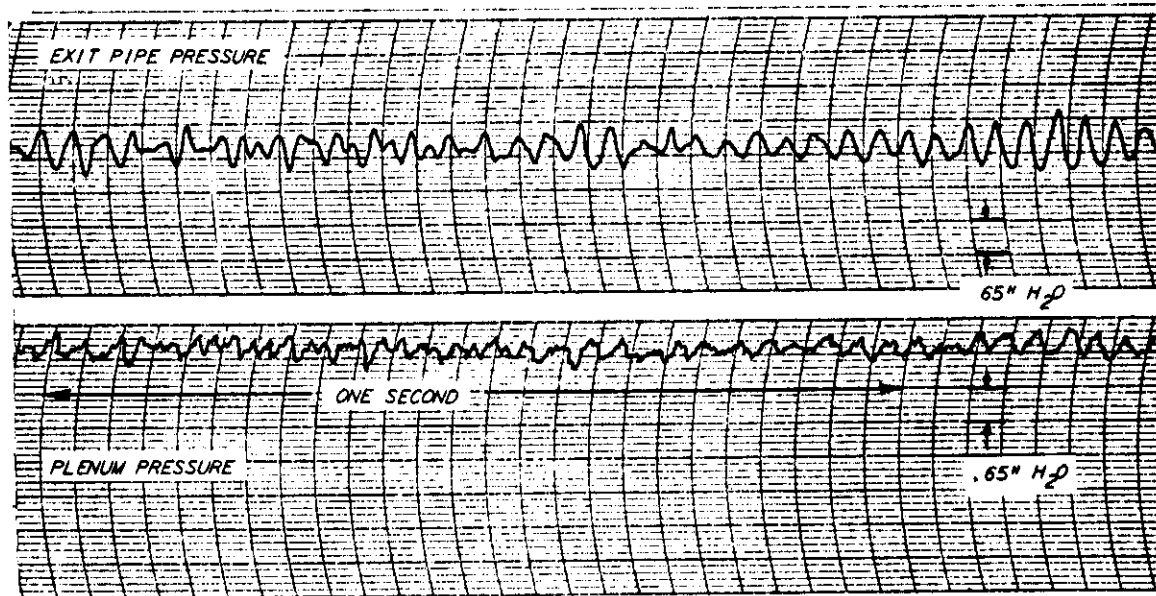


UNITS: SUCTION RATE TO REMOVE NORMAL BOUNDARY LAYER AT ONE SLOT (1.25 FT³/SEC)
FIGURE 16 PRESSURE RECOVERY IN DIFFUSER



PLENUM VOLUME, $V = 3.54 \text{ FT.}^3$
 TUNNEL VELOCITY, $U_0 = 200 \text{ FT/SEC}$
 BOUNDARY LAYER SHAPE PARAMETER, $H = 2.0$ (TURBULENT BOUNDARY LAYER)
 NO SPLITTERS

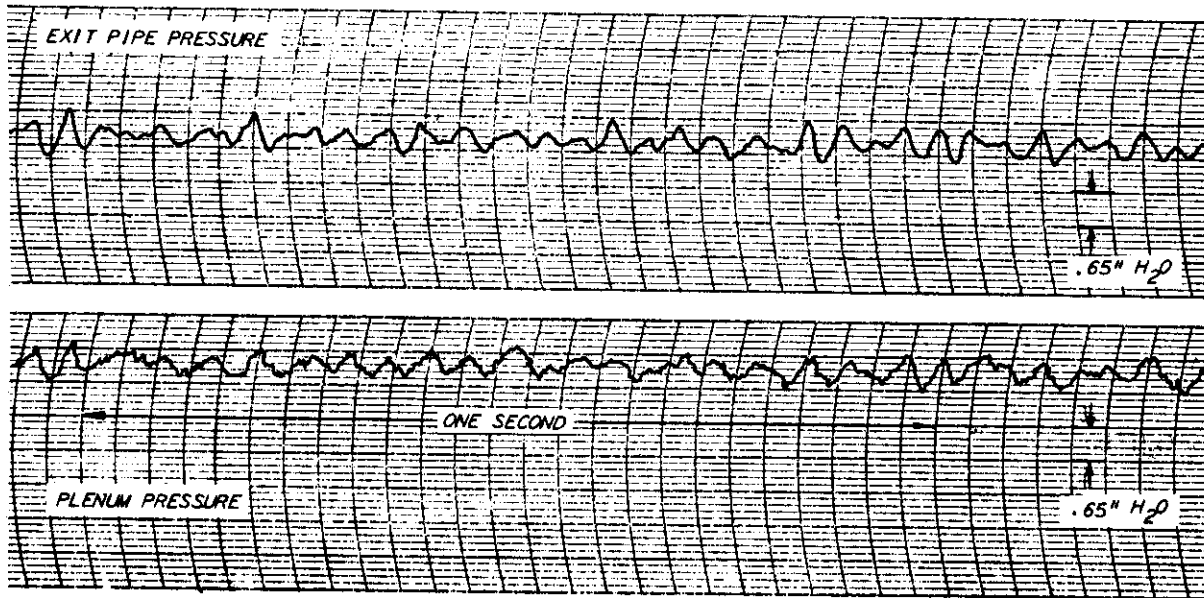
FIGURE 17a



PLENUM VOLUME, $V = 1.4 \text{ FT.}^3$
 TUNNEL VELOCITY, $U_0 = 200 \text{ FT/SEC}$
 BOUNDARY LAYER SHAPE PARAMETER, $H = 2.0$ (TURBULENT BOUNDARY LAYER)
 NO SPLITTERS

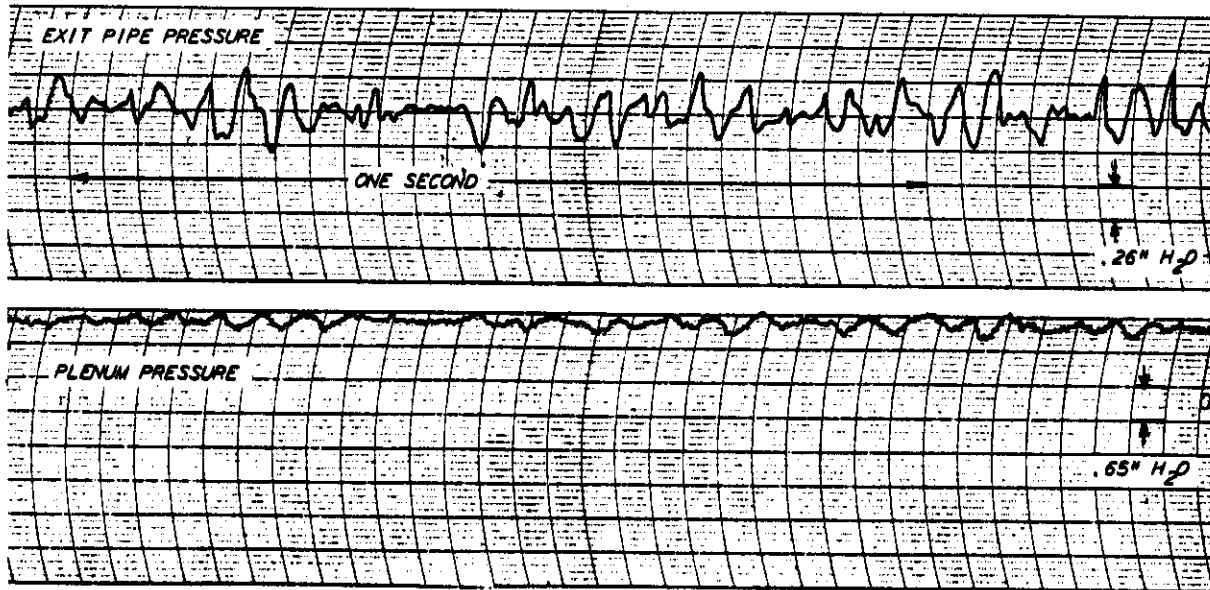
FIGURE 17b PRESSURE VARIATIONS WITH TIME
 (SUCTION APPLIED TO BOUNDARY LAYER)

Contrails



PLENUM VOLUME, $V = 3.54 \text{ FT.}^3$
 TUNNEL VELOCITY, $U_0 = 200 \text{ FT/SEC}$
 BOUNDARY LAYER SHAPE PARAMETER, $H = 2.9$ (LAMINAR LIKE BOUNDARY LAYER)
 NO SPLITTERS

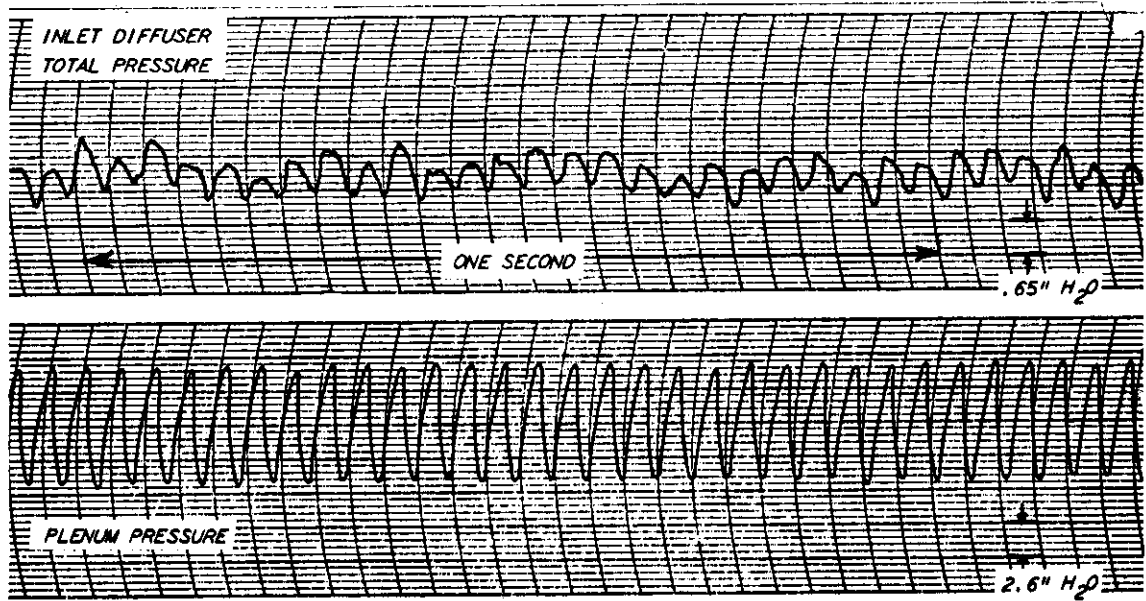
FIGURE 17c



PLENUM VOLUME, $V = 3.54 \text{ FT.}^3$
 TUNNEL VELOCITY $U_0 = 200 \text{ FT/SEC}$
 BOUNDARY LAYER SHAPE PARAMETER, $H = 2.0$ (TURBULENT BOUNDARY LAYER)
 SPLITTERS INSERTED

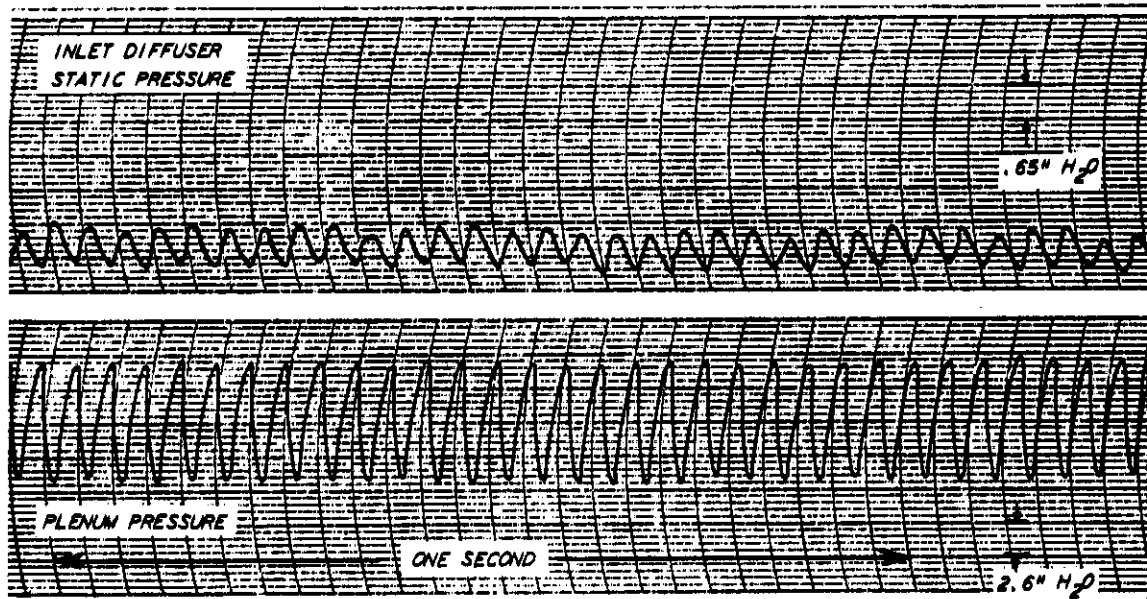
FIGURE 17d PRESSURE VARIATIONS WITH TIME
 (SUCTION APPLIED TO BOUNDARY LAYER)

Contrails



PLENUM VOLUME, $V = 3.54 \text{ FT.}^3$
 TUNNEL VELOCITY, $U_0 = 200 \text{ FT/SEC}$
 BOUNDARY LAYER SHAPE PARAMETER, $H = 2.0$ (TURBULENT BOUNDARY LAYER)
 NO SPLITTERS

FIGURE 18a



PLENUM VOLUME, $V = 3.54 \text{ FT.}^3$
 TUNNEL VELOCITY $U_0 = 200 \text{ FT/SEC}$
 BOUNDARY LAYER SHAPE PARAMETER, $H = 2.0$ (TURBULENT BOUNDARY LAYER)
 NO SPLITTERS

FIGURE 18b PRESSURE VARIATIONS WITH TIME
 (SUCTION APPLIED TO BOUNDARY LAYER)